Cell



# Gasdermin D licenses MHCII induction to maintain food tolerance in small intestine

## Graphical abstract

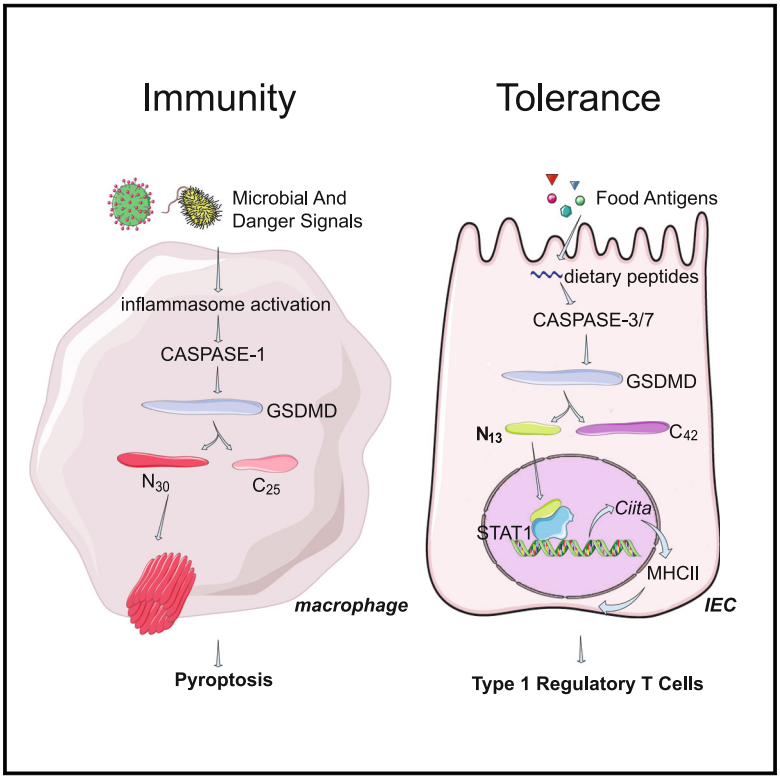


## Highlights

- Dietary antigens induce a non-pyroptotic 13kD GSDMD fragment in the upper small intestine
- Caspase-3 and -7 cleave GSDMD at D88 in duodenum IECs in response to dietary antigens
- Nuclear-localized GSDMD fragment regulates CIITA and MHCII in IECs to induce Tr1 cells
- Inactivation of food-induced GSDMD cleavage in IECs disrupts immune tolerance to food

## Authors

Kaixin He, Tingting Wan, Decai Wang, ..., Zhigang Tian, Richard A. Flavell, Shu Zhu

## Correspondence

richard.flavell@yale.edu (R.A.F.), zhushu@ustc.edu.cn (S.Z.)

## In brief

Dietary-antigen-dependent cleavage of Gasdermin D maintains food tolerance irrespective of pyroptosis.

He et al., 2023, Cell *186*, 3033–3048
July 6, 2023 
https://doi.org/10.1016/j.cell.2023.05.027

CellPress

Cell

CellPress

Article

# Gasdermin D licenses MHCII induction to maintain food tolerance in small intestine

Kaixin He,[1,2,7] Tingting Wan,[2,7] Decai Wang,[2,7] Ji Hu,[1,2,7] Tingyue Zhou,[2] Wanyin Tao,[2] Zheng Wei,[3] Qiao Lu,[3] Rongbin Zhou,[2,4] Zhigang Tian,[2,4] Richard A. Flavell,[3,5,*] and Shu Zhu[1,2,4,6,8,*]

[1]Department of Digestive Disease, The First Affiliated Hospital of USTC, Division of Life Sciences and Medicine, University of Science and Technology of China, Hefei 230001, China

[2]Institute of Immunology and the CAS Key Laboratory of Innate Immunity and Chronic Disease, Division of Life Sciences and Medicine, University of Science and Technology of China, Hefei 230027, China

[3]Department of Immunobiology, Yale University School of Medicine, New Haven, CT 06520, USA

[4]Institute of Health and Medicine, Hefei Comprehensive National Science Center, Hefei 230601, China

[5]Howard Hughes Medical Institute, Yale University School of Medicine, New Haven, CT 06520, USA

[6]School of Data Science, University of Science and Technology of China, Hefei 230026, China

[7]These authors contribute equally

[8]Lead contact

*Correspondence: richard.flavell@yale.edu (R.A.F.), zhushu@ustc.edu.cn (S.Z.)

https://doi.org/10.1016/j.cell.2023.05.027

## SUMMARY

The intestinal epithelial cells (IECs) constitute the primary barrier between host cells and numerous foreign antigens; it is unclear how IECs induce the protective immunity against pathogens while maintaining the immune tolerance to food. Here, we found IECs accumulate a less recognized 13-kD N-terminal fragment of GSDMD that is cleaved by caspase-3/7 in response to dietary antigens. Unlike the 30-kD GSDMD cleavage fragment that executes pyroptosis, the IEC-accumulated GSDMD cleavage fragment translocates to the nucleus and induces the transcription of CIITA and MHCII molecules, which in turn induces the Tr1 cells in upper small intestine. Mice treated with a caspase-3/7 inhibitor, mice with GSDMD mutation resistant to caspase-3/7 cleavage, mice with MHCII deficiency in IECs, and mice with Tr1 deficiency all displayed a disrupted food tolerance phenotype. Our study supports that differential cleavage of GSDMD can be understood as a regulatory hub controlling immunity versus tolerance in the small intestine.

## INTRODUCTION

The loss of normal immune tolerance to food is most obviously associated with food allergies (e.g., peanut, egg, and milk) and celiac diseases. It is unclear how protective immunity is induced against pathogens while still maintaining immune tolerance to food, and a deeper understanding of these processes should facilitate development of treatments against infection, inflammation, and allergy conditions in the intestine. Studies of immune tolerance have focused extensively on commensal bacteria in the large intestine and have implicated induction of T cells with regulatory functions by antigen-presenting cells, such as $CD103^+$ dendritic cells (DC) and ILC3s,[1–3] the mechanisms of immune tolerance to food are less studied. A seminal study established that dietary antigens induce immune tolerance by sustaining regulatory T cells in the intestine,[4] and food-antigen-specific T cells tend to form a set of hyporesponsive T helper cell subsets lacking the inflammatory functions.[5] Besides typical antigen presenting cells such as DC, intestinal epithelial cells (IECs) are reported to shape the regulatory $IL10^+CD4^+$ T cell populations in the small intestine as well.[6–11] However, how signals transduced in IECs induce the immune tolerance to food remains unknown.

Cleaved Gasdermin D (GSDMD) is the executioner protein of pyroptosis, a lytic form of cell death that initiates suicide of the cell, an essential aspect of immune defenses against foreign antigen.[12–14] Previous studies have investigated the role of GSDMD in myeloid cells such as macrophages and DC.[12–18] However, despite public expression data and our own observations of very high GSDMD expression in IECs (Figures S1A and S1B), only a few studies have examined GSDMD's potential roles in IECs, which showing the death-promoting or cytokine-release functions as induced by microbes or danger signals, in distal small intestine and colon.[19–22]

However, here in upper small intestine, we found IECs accumulate an unexpected 13kD fragment of GSDMD that is cleaved by caspase-3/7 in response to proteinaceous dietary antigens. The 13kD N-terminal GSDMD cleavage fragment translocates to the nucleus, where it induces the transcription of CIITA and major histocompatibility complex class II (MHCII) molecules in IECs, which, in turn, induces the Type 1 regulatory T cells to maintain the immune tolerance to food. The mice carried the small intestine cleavage-resistant variant of GSDMD disrupts

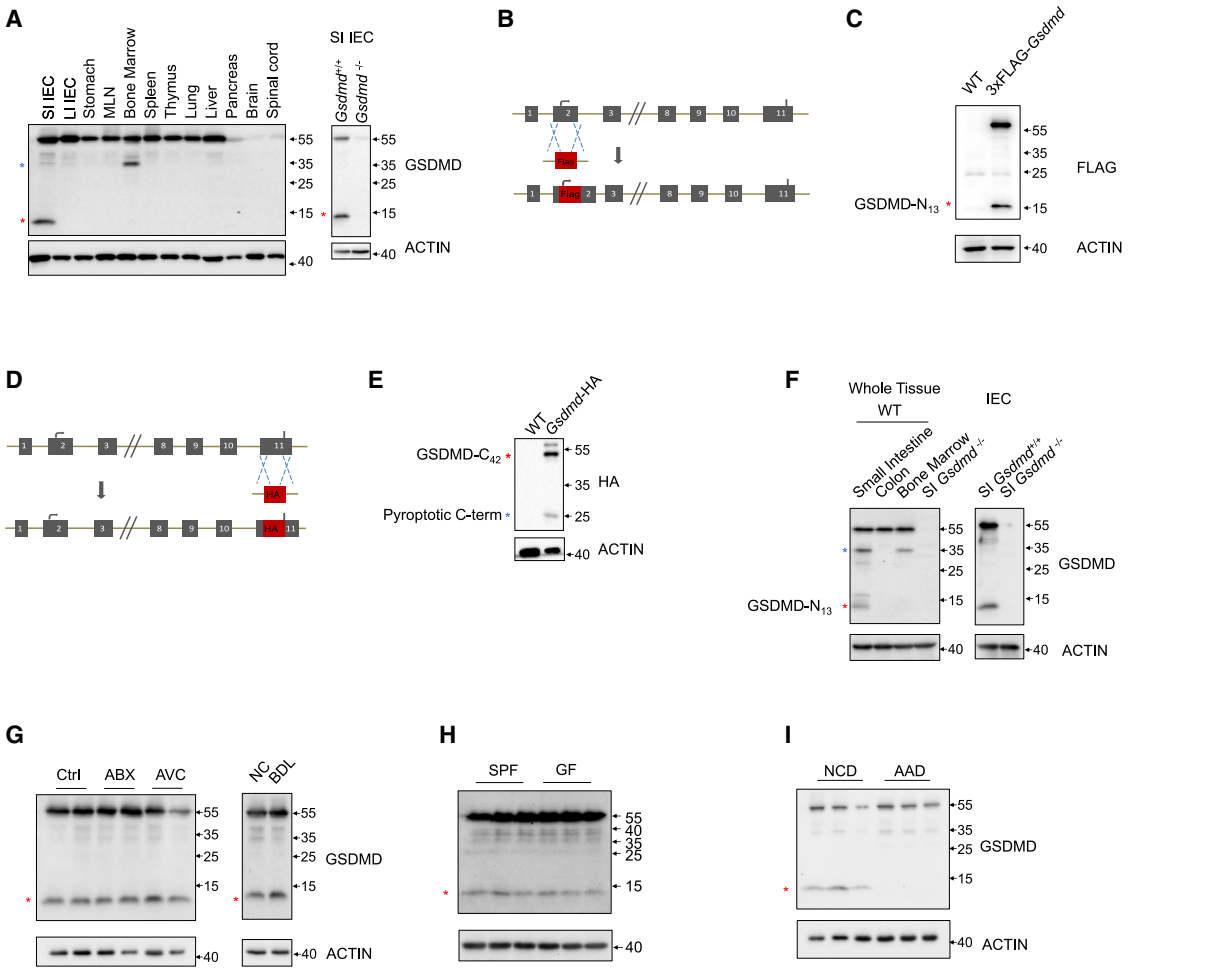


**Figure 1. Dietary antigens induce a non-pyroptotic 13kD GSDMD fragment in the upper small intestine**

(A) GSDMD fragments in various tissues or cells. Western blots (WB) showing bands at 13 kDa (red star) or 30 kDa (blue star) using anti-GSDMD antibody (ab219800) in extracts from the indicated tissues, small intestine (SI) IEC lysates of *Gsdmd*$^{-/-}$mice were used to verify the specificity of the antibody.

(B and D) Illustration of the CRISPR-Cas9 strategy to generate 5′3xFLAG-*Gsdmd* mice and (B) Gsdmd-3'HA mice (D).

(C and E) Western blots showing a 13-kD GSDMD band (GSDMD-$N_{13}$, red star) in extracts prepared from isolated IECs from 5′FLAG-*Gsdmd* mice (C) and a 42KD GSDMD band (GSDMD-$C_{42}$, red star) in isolated IECs from Gsdmd-3'HA mice (E).

(F) Western blots of different GSDMD cleavage fragments in indicated tissues or cells.

(G–I) Western blots detection of GSDMD fragments in IECs from mice treated with antibiotics (ABX) or anti-viral cocktails (AVC), mice given bile duct ligation (BDL) surgery, or controls (G); in IECs from germ free (GF) mice or specific pathogen free (SPF) mice (H); in IECs from mice fed with amino acid diet (AAD) devoid of proteins or normal chow diet (NCD).

(A, C, and E–I) are representative of at least three experiments. Red star: GSDMD-$N_{13}$ or GSDMD-$C_{42}$; blue star: GSDMD-$N_{30}$.

See also Figure S1.

the immune tolerance to food but does not affect pyroptosis, suggesting an essential role of GSDMD in food tolerance that is distinguished from GSDMD's canonical role to mediate inflammatory pyroptosis, which is mediated by caspase-1/11 in responds to microbial or danger signals.

## RESULTS

### Dietary antigens induce a non-pyroptotic 13-kD GSDMD fragment in the small intestine

We began our investigation of potential regulation and activation of GSDMD in IECs isolated from the intestine, stomach, lymphoid tissues (mesenteric lymph node, bone marrow [BM], spleen, and thymus), and other organs, including the lung, liver, pancreas, brain, and spinal cord. Homogenates from the intestine, stomach, lymphoid tissues, lung, and liver that we checked with immunoblotting accumulated the full-length form of GSDMD (~55 kD), and we detected the previously identified inflammatory cleaved forms of GSDMD (~30 kD N terminus (GSDMD-$N_{30}$)[12–14] in both small intestine and BM using a commercial anti-GSDMD antibody. To our surprise, we observed an unexpected ~13-kD GSDMD band in the small intestine IEC samples (Figure 1A). Moreover, as the signals for the ~13-kD band was much stronger than the bands for the previously

reported 30-kD inflammatory cleaved form (Figures 1A and S1C), we wondered whether GSDMD may function in some non-pyroptotic role in the small intestine.

To support further investigations of this 13-kD GSDMD fragment, we generated two GSDMD knockin mouse lines in which we fused a FLAG-tag to the N terminus or a HA-tag to the C terminus of GSDMD (Figures 1B and 1D). Our observation of similarly sized ~13-kD GSDMD band (GSDMD-$N_{13}$) and a corresponding GSDMD C terminus fragment (GSDMD-$C_{42}$) in the upper small intestines of these tagged GSDMD knockin mouse lines (Figures 1C and 1E), supported the potential cleavage of GSDMD into 13- and 42-kD fragments. We next examined dissected intestine tissues and IECs isolated from the upper small intestine: there was a strong signal for the inflammatory cleaved form of GSDMD (GSDMD-$N_{30}$) in the intestine tissues but barely any signal in IECs. In sharp contrast, the signals for the GSDMD-$N_{13}$ fragment were dominant in the IECs (Figure 1F). In consistency, we also stained against the active form of caspase (CASP)-1—the known protease for pyroptotic cleavage of GSDMD into 30- and 25-kD fragments[13,14])—and detected a much stronger signal in the small intestine tissue samples than the IECs (Figure S1D). These data suggest a CASP1-mediated 30/25 pyroptotic cleavage of GSDMD in the non-IECs, whereas a potential 13/42 cleavage of GSDMD in IECs with unknown trigger and function in the upper small intestine.

To explore potential triggers of the apparent 13/42 cleavage of GSDMD in the upper small intestine, we sequentially depleted individual environmental components from the intestine. First, given that bacteria such as *Salmonella typhimurium* and viruses (e.g., rotavirus) are known to induce the 30/25 cleavage of GSDMD,[20,23] we tested whether intestinal commensal bacteria and/or viruses are required for the induction of 13/42 cleavage of GSDMD. As the distribution of GSDMD-$N_{13}$ and full-length GSDMD in isolated IECs was unaffected by treatment with antibiotics (ABX) or by anti-viral cocktails (AVCs), we infer that it is not commensal bacteria or commensal viruses per se that trigger the observed 13/42 cleavage (Figures 1G, S1E, and S1F). We also detected the GSDMD-$N_{13}$ fragment in germ-free mice (i.e., lacking bacteria), as well as in pathogen-infected mice (with *Citrobacter rodentium* or *Listeria monocytogenes*). Neither condition affected the distribution of GSDMD-$N_{13}$ and full-length GSDMD (Figures 1H and S1H). Bile acids are known to regulate inflammasome activation[24]; yet, we observed no effect on the distribution of GSDMD-$N_{13}$ and full-length GSDMD when bile acids were removed from the intestinal tract by bile duct ligation (BDL) surgery (Figures 1G and S1G). These data indicate that the 13-kD GSDMD fragment is not induced by microbial signals or bile acids.

Given that the GSDMD-$N_{13}$ fragment was evident in the upper small intestine but not in other examined tissues, and considering the abundance of nutrients present at this location of the digestive tract, we reasoned that food component(s) might induce this fragment. Supporting this idea, a screen based on feeding mice with diverse types of diet revealed that animals given standard chow had significantly higher levels of GSDMD-$N_{13}$ compared with animals given an amino acid diet (AAD) devoid of intact proteins (Figure 1I), which is specifically formulated to lack proteinaceous dietary antigens.[4] Importantly, we experimentally confirmed in the IECs that the distribution of GSDMD-$N_{13}$ and full-length GSDMD was unaffected by deficiency of inflammasome components (Figure S1I), confirming that the induction of this cleavage is an inflammasome-independent process. Thus, our results collectively support that proteinaceous dietary antigens but not commensals induce a non-pyroptotic 13-kD GSDMD fragment in epithelial cells of the upper small intestine.

## Caspase-3 and caspase-7 cleave GSDMD at D88 in IECs in response to dietary antigens

We next performed immunoprecipitation followed by mass spectrometry (IP-MS) to identify potential protease(s) responsible for the 13/42 cleavage of GSDMD. We incubated a purified recombinant GST-tagged GSDMD protein with IEC protein lysates, followed by IP-MS with beads coated with anti-GST antibodies; or performed IP-MS with beads coated with anti-FLAG antibodies in lysates from HEK293T cells that transfected with FLAG-tagged *Gsdmd* plasmids. By analyzing the MS results, known proteases such as caspase (CASP)-3, CASP-7, and CASP-1 were identified as top candidates of the indicated gel band from the Coomassie-stained SDS-PAGE (Figures 2A, 2B, and S2A; Table S1). Given that CASP-1, CASP-3, and CASP-7 are reported to cleave GSDMD in macrophages,[13,14,25–29] we assessed whether the 13/42 GSDMD fragmentation we observed in IECs is mediated by enzymatic cleavage using these three GSDMD proteases in IECs and in BM cells. Whereas CASP-1 showed moderate activation in BM cells (where we detected abundant 30/25 GSDMD cleavage) but showed only weakly activation in IECs, we found that CASP-3 and CASP-7 were strongly activated in IECs but not in BM cells (Figure 2C). We also found that CASP-3 and CASP-7 activation (as well as GSDMD-$N_{13}$ fragment) occurred in the upper small intestine—including duodenum and jejunum—a region replete with food antigens—but not in the distal small intestine or colon (Figure 2D), findings supporting a link between dietary antigens, CASP-3/7 activation, and potential 13/42 GSDMD cleavage.

Indeed, overexpression of CASP-7 or CASP-3 led to 13/42 GSDMD cleavage in HEK293T cells, whereas overexpression of CASP-1 caused the expected pyroptotic 30/25 cleavage (Figures 2E and S2B). No GSDMD-$N_{13}$ fragment was detected upon treating HEK-293T cells co-expressing GSDMD and CASP-7 with the CASP-3/7 inhibitor Ac-DEVD-CHO (Figure 2F). Further, an *in vivo* experiment showed that intraperitoneal injection of Ac-DEVD-CHO for 4 days reduced the activation of CASP-3 and CASP-7, as well as the extent of 13/42 N-terminal cleavage of GSDMD in IECs from upper small intestine (Figure 2G), confirming that CASP-3 and CASP-7 are proteases capable of catalyzing 13/42 GSDMD cleavage both *in vitro* and *in vivo*.

Notably, although GSDMD and CASP-3/7 were all highly expressed in both small intestine and colon, we only observed strong CASP-3/7 activation and 13/42 GSDMD cleavage in the upper small intestine (Figure 2D). We therefore asked whether dietary antigens can explain this activation pattern: indeed, depletion of food antigens by feeding the mice with the aforementioned AAD led to reductions in both CASP-3/7 activation and 13/42 cleavage of GSDMD in IECs (Figure 2H). Further, incubation of the lysates of HEK-293T cells overexpressed with myc-tagged *Casp7* and FLAG-tagged *Gsdmd* together

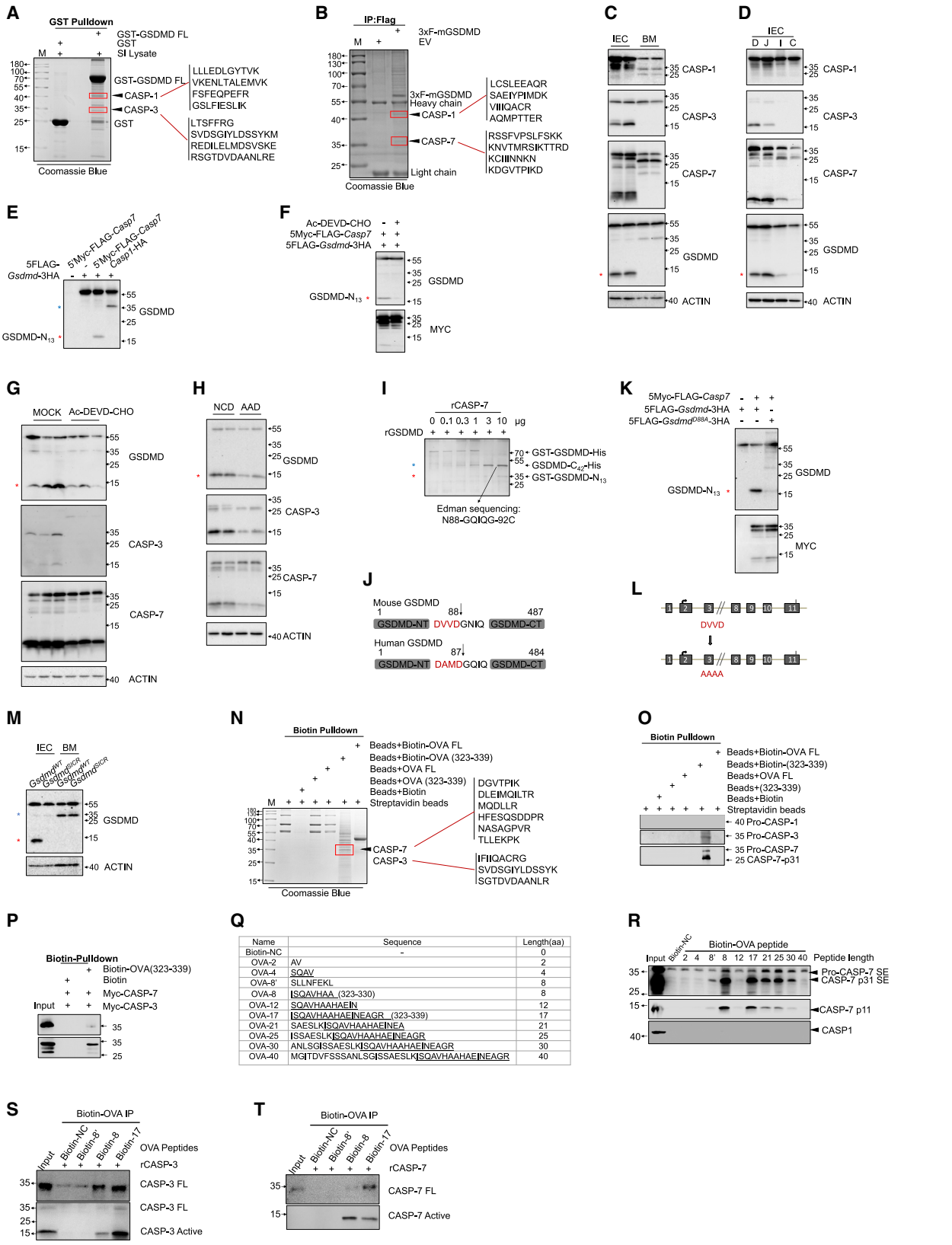


*(legend on next page)*

with small intestine IEC cell lysates, resulted in CASP-7 activation and 13/42 cleavage of GSDMD; however, when we replaced the small intestine IEC cell lysates from normal chow diet (NCD)-fed mice with that from AAD-fed mice, the activation of CASP-7 and 13/42 cleavage of GSDMD was abolished (Figure S2C). These results indicate that dietary antigens absorbed in IECs may induce the CASP-3/7 activation as well as the 13/42 cleavage of GSDMD.

We next performed the *in vitro* caspase-mediated GSDMD cleavage experiments, the recombinant human CASP-3 or CASP-7 but not CASP-1 can induce the 13/42 cleavage of GSDMD (Figure S2D), and the recombinant human CASP-7 induce the 13/42 cleavage of GSDMD in a dose-dependent manner (Figure 2I). Then we subjected the GSDMD-$C_{42}$ for the Edman N-terminal sequencing to identify the exact cleavage site (Figure 2I). The result showed that recombinant human CASP-3 or CASP-7 cleaved recombinant human GSDMD protein at D87 (Figure 2I).[25] The corresponding residue in mouse is D88 which is positioned in a classic caspase substrate Asp-Val-Val-Asp (DVVD) motif (Figure 2J), findings in line with the previous reports showing CASP-3/7 cleave GSDMD in D88 in mouse macrophages.[25–30] We further validated the cleavage bands we detected in different tissues or HEK293T cells transfected with plasmids expressing GSDMD truncations by GSDMD antibodies or FLAG/HA tag antibodies, showing that anti-GSDMD (ab219800) targets GSDMD-N1-88 (Figures S2E–S2G).

We generated a variant of GSDMD with DVVD to AAAA mutation, assays GSDMD cleavage in HEK293T cells or in small intestine cleavage-resistant variant (*Gsdmd*$^{SICR}$) knockin mice and experimentally confirmed that this GSDMD variant is resistant to CASP-7-mediated cleavage (Figures 2K–2M). Note that pyroptotic cleavage of GSDMD or pyroptotic cytokine secretion was not affected in *Gsdmd*$^{SICR}$ knockin mice (Figures 2M, S2H, and S2I), suggesting that 13/42 cleavage might not inactivate pyroptosis in IECs *in vivo*. Moreover, the IECs from *Gsdmd*$^{SICR}$ knockin mice showed similar apoptosis level in comparison to the littermate WT mice (Figure S2J), indicating that 13/42 cleavage of GSDMD does not affect IEC death, in line with the finding that the AAD feeding does not affect IEC death (Figure S2K). These results suggest CASP-3 and CASP-7 cleave murine GSDMD at 85-DVVD-88 in the upper small intestine, and the *Gsdmd*$^{SICR}$ mice affect only 13/42 cleavage but not pyroptotic cleavage of GSDMD.

Next, we sought to determine how proteinaceous dietary antigens induce the 13/42 cleavage of GSDMD. We performed IP-MS unbiasedly to identify interaction partner proteins of dietary antigens. After exposing the protein lysates from upper small intestine to commercially available biotin-labeled synthetic full-length ovalbumin (OVA-FL) or ovalbumin peptide 323–339 (OVA [323–339]), we immunoprecipitated the potential OVA-peptide-binding proteins with streptavidin beads and performed MS for Coomassie-stained promising gel band (Figure 2N).

Interestingly, both CASP-3 and CASP-7 (Figures 2N and S2A; Table S1) are top candidates that are pulled downed by Biotin-OVA (323–339) peptide-an H-2b-restricted OVA class II epitope, but not the full-length OVA, bring our attention to the potential correlation of this binding with the antigen presentation process, which we will discuss later. We further confirmed the interaction by IP with biotin-labeled OVA peptides, incubated with either IEC protein lysates or HEK293T cells lysates, and immunoblotted with different CASPs. We found that Biotin-OVA (323–339) peptide strongly interact with CASP-3 and 7, but not CASP-1 (Figures 2O and 2P), suggesting dietary peptides and CASP3/7 form a complex to induce 13/42 cleavage of GSDMD. Further, we tested the properties of the peptides that binds to and activate CASP-7. Notably, OVA peptides with length of 8 and 17 aa strongly bind and induce CASP-7 cleavage, OVA peptides with length of 21, 25, and 30 aa weakly bind and activate CASP-7, whereas OVA peptides with length of 2, 4, 12, and 40 aa could not bind and activate CASP-7 (Figures 2Q, 2R, S2L, and S2M). Although it is not completely clear of the peptidomics in IECs, and it is also not clear the sequence characteristics of the peptides that may activate

**Figure 2. Caspase-7 and caspase-3 cleave GSDMD at D88 in duodenum IECs in response to dietary antigens**

(A and B) GST-GSDMD pull-down in small intestine IEC lysates (A); FLAG-GSDMD pull-down in HEK293T cell lysates (B). The red box indicates Coomassie-brilliant-blue-stained band that subject for LC-MS/MS analysis and peptide sequences are shown.

(C and D) Western blots for anti-CASP1, CASP-3, CASP-7, and GSDMD in IECs from upper small intestine and bone marrow (BM) (C) or IECs from the indicated sections of the intestine (D).

(E) The induction of GSDMD-$N_{13}$ fragment by CASP-7 in HEK293T cells.

(F) CASP-3/7 inhibitor prevent the induction of GSDMD-$N_{13}$ fragment in HEK293T cells.

(G and H) Western blots for CASP-1, CASP-3, CASP-7, and GSDMD in duodenum IECs from mice intraperitoneally injected with CASP3/7 inhibitor (G) or mice fed with AAD (H).

(I) *In vitro* cleavage assay of GSDMD by recombinant CASP-7 in different concentration, the GSDMD-$C_{42}$ fragment was subjected to Edman sequencing.

(J) Cleavage site of human and mouse GSDMD by CASP-3/7.

(K) Cleavage assay in cells transfected with GSDMD D88A mutant plasmid that resistant to CASP-3/7 cleavage.

(L) Illustration of the CRISPR-Cas9 strategy to generate the *Gsdmd*$^{SICR}$ mutant variant mice with Alanine substitutions at the four residues comprising the putative CASP-7-cleavage motif-DVVD (*Gsdmd*$^{SICR}$; SICR: small intestine cleavage resistant mutant).

(M) GSDMD cleavage in duodenum IECs or BM cells from *Gsdmd*$^{SICR}$ mutant mice.

(N) Biotin-OVA (full-length/323–339-aa peptide) pull-down in small intestine IEC lysates.

(O) Interaction between OVA peptides and CASP-1/3/7 in intestine.

(P) Interaction between OVA peptides and CASP-3/7 overexpressed in HEK293T cells.

(Q) OVA peptides sequences used in Figures 2R–2T and S2L–S2M.

(R) Mapping of biotin-OVA peptides that bind to and activating CASP-7 in IECs.

(S and T) Validation of biotin-OVA peptides that bind to and activating purified recombinant CASP-3 or CASP-7 protein.

Data in (E–I), (K), (M), (O), (P), and (R–T) are representative of at least three experiments.

See also Figure S2 and Table S1.

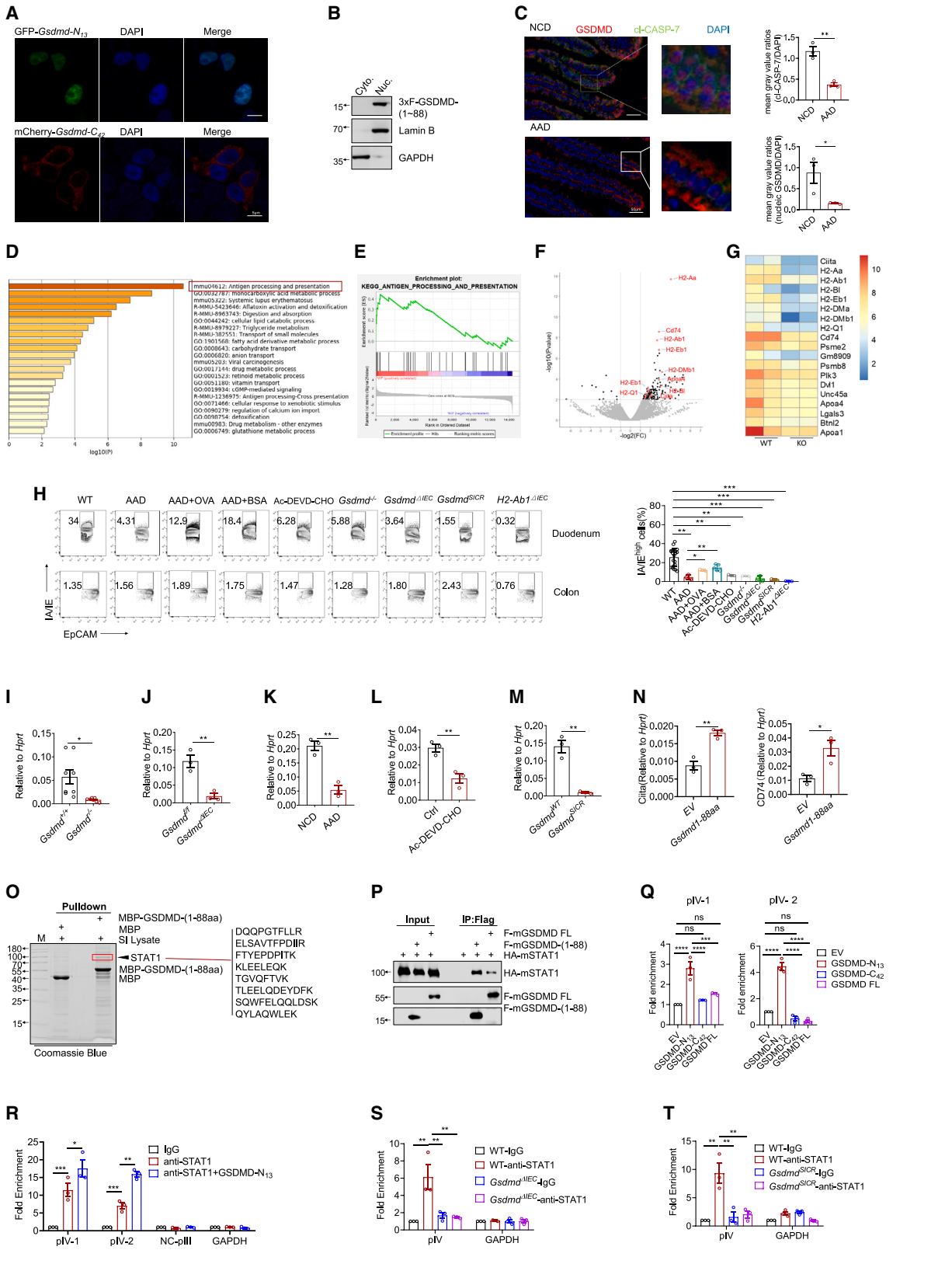


(legend on next page)

CASP-3/7 as well as the 13/42 cleavage of GSDMD, we noticed that a previous report showing peptides with specific motif directly activate apoptotic caspase[31]; in agreement with that, by co-incubating purified recombinant CASP-3/7 proteins with synthesized Biotin-OVA peptides and pulled down with streptavidin beads, we found OVA peptides with length of 8 and 17 aa directly bind and activate CASP-3/7 (Figure 2S and 2T). These results indicate that dietary peptides directly bind and activate CASP-3 and CASP-7 to induce the 13/42 cleavage of GSDMD.

## The nuclear-localized GSDMD fragment assists STAT1 to induce CIITA and MHCII in IECs

We next investigated potential physiological consequences of the 13/42 GSDMD cleavage in IECs. We first generated truncation fragments of recombinant GSDMD including the GSDMD-$N_{13}$ cleaved in response to food antigens (1–88 aa), as well as corresponding GSDMD-$C_{42}$ fragment (89–487 aa). We then examined the subcellular localizations of these recombinant GSDMD truncation variants: GSDMD-$C_{42}$ was localized in the cytosol (Figures 3A and S3A). To our surprise, unlike GSDMD-$N_{30}$, which localizes at the membrane where it initiates pyroptosis,[15,32] GSDMD-$N_{13}$ was localized in the nucleus (Figures 3A, 3B, and S3A). Further, upon replacing normal chow with the aforementioned AAD, we detected a significant reduction in the extent of nuclear-localized GSDMD fragment in IECs, as well as CASP-7 activation (Figures 3C and S3B–S3D), suggesting a food-antigen-induced nuclear translocation of the GSDMD-$N_{13}$.

Because there is no putative nuclear localization signal (NLS) in GSDMD-$N_{13}$ according to NLS prediction tools, including cNLS Mapper, PredictNLS, DeepLoc-1.0, PSORT, NLStradamus (Figure S3E), and, indeed, we detected no interactions between GSDMD-$N_{13}$ and importins (Figures S3F and S3G), we reasoned that GSDMD-$N_{13}$ may translocate into the nucleus through an Importin-independent way.

After initially excluding the involvement of importins in dietary-antigen-induced nuclear translocation of GSDMD-$N_{13}$ (Figures S3E–S3G), we used a purified recombinant MBP-tagged GSDMD-$N_{13}$ truncation protein for IP/MS with small intestinal cell extracts to identify potential binding proteins that assist GSDMD-$N_{13}$'s nuclear translocation. We identified multiple nucleoporins (e.g., Nup155, Nup107, and Nup98) (Figures S2A and S3H); proteins of this family have been reported to function in the nuclear translocation of diverse signaling proteins (e.g., β-catenin and Smad3/4).[33–35] We confirmed the interaction between GSDMD-$N_{13}$ and three nucleoporins (Nup155, Nup107, and Nup98) by coIP (Figure S3I). Further, in comparison with almost complete nuclear localization of GSDMD-$N_{13}$ in control HEK293T cells, we found that simultaneously knocking down three nucleoporins (Nup155, Nup107, and Nup98) results in significantly shifted cytoplasmic/nuclear distribution of GSDMD-$N_{13}$ in HEK293T cells (Figure S3J), indicating nucleoporins assist the nuclear translocation of GSDMD-$N_{13}$.

We then explored which pathway(s) may be affected by nuclear GSDMD-$N_{13}$ in IECs by generating three mouse lines: GSDMD complete knockout mice (*Gsdmd*$^{-/-}$), mice specifically deficient for GSDMD in IECs (*Gsdmd*$^{\Delta IEC}$), and mice harboring the small intestinal 13/42 cleavage-resistant GSDMD variant (*Gsdmd*$^{SICR}$ mice). We first analyzed the transcriptome of IECs from the upper small intestine of *Gsdmd*$^{-/-}$ and littermate WT mice. Gene ontology (GO) analysis indicated enrichment in IECs for differentially regulated genes with annotations relating to antigen processing and presentation, with particularly strong enrichment for genes encoding major histocompatibility complex class II (MHCII) molecules, as well as *Ciita* (Figures 3D–3G), which is widely understood as a "master control factor" for the expression of MHCII molecules.[36]

We next used FACS and qPCR to measure the expression levels of MHCII molecules and CIITA in FACS-sorted IECs from *Gsdmd*$^{-/-}$ and *Gsdmd*$^{\Delta IEC}$ mice, in comparison with their WT littermates. Need to mention that our IA/IE FACS staining experiments were normally carried out at the afternoon when the IA/IE expression in IECs are lowest among a day (Figures S3K and

**Figure 3. The nuclear-localized GSDMD fragment assists STAT1 to induce CIITA and MHCII in IECs**

(A and B) GSDMD-$N_{13}$ locates in nucleus. Confocal images of HeLa cells transfected with indicated florescence-fused GSDMD fragments (A). Western blot of nuclear and cytoplasmic extracts of HEK293T cells transfected with 3xFLAG-*Gsdmd* plasmid (B).

(C) Food antigen induces CASP-7 activation and nucleic localization of GSDMD. Immunofluorescence for GSDMD and cleaved-CASP-7 in upper small intestine sections from mice fed with NCD or AAD, and quantification of cleaved-CASP-7 and nuclear localization of GSDMD-$N_{13}$ in IECs.

(D–G) RNA sequencing of IECs from *Gsdmd*-knockout (KO) mice compared with that from WT littermates. Gene ontology analysis of downregulated genes (D). Gene set enrichment analysis (GSEA) analysis of antigen presentation pathway (E). Volcano Plot of differentially regulated genes, with downregulated genes belongs to antigen presentation pathway labeled in red (F). Heatmap showing the expression levels of downregulated antigen presentation related genes (G).

(H) Representative FACS staining of MHCII expression in IECs of duodenum or colon from the indicated mouse strains or treated mice, and quantification of MHCII-expressing IECs in duodenum.

(I–M) qPCR analysis of *Ciita* transcripts in duodenum IECs from *Gsdmd*$^{KO}$ mice (I), *Gsdmd*$^{\Delta IEC}$ mice (J), AAD-treated mice (K), Ac-DEVD-CHO-treated mice (L), or *Gsdmd*$^{SICR}$ mutant variant mice (M).

(N) qPCR analysis showing *Ciita* and MHCII induction in MC38 cells.

(O) MBP-GSDMD pull-down in small intestine IEC lysates.

(P) CoIP assay in HEK293T cells transfected with STAT1 and GSDMD truncation plasmids.

(Q) ChIP-qPCR assay detecting the binding of GSDMD to *CIITA* promoter IV in 293T cells.

(R) ChIP-qPCR assay detecting the synergistic binding between GSDMD and STAT1 to *CIITA* promoter IV in HEK293T cells.

(S and T) ChIP-qPCR assay detecting the effects of GSDMD deficiency (S) or GSDMD mutation (T) on the binding of STAT1 to *Ciita* promoter IV in IEC Lysates from *Gsdmd*$^{\Delta IEC}$ mice (S) or *Gsdmd*$^{SICR}$ mice(T), and corresponding littermate WT mice.

In (C), (H–N), and (Q–T), data are presented as the mean ± SEM. For comparisons between two groups, Student's t tests were used; for more than two groups, analysis of variance (ANOVA) was used; ns, not significant, *$p < 0.05$, **$p < 0.01$, ***$p < 0.001$, and ****$p < 0.0001$.

(A–C, H–N, and P–T) are representative of at least three experiments.

See also Figure S3 and Table S1.

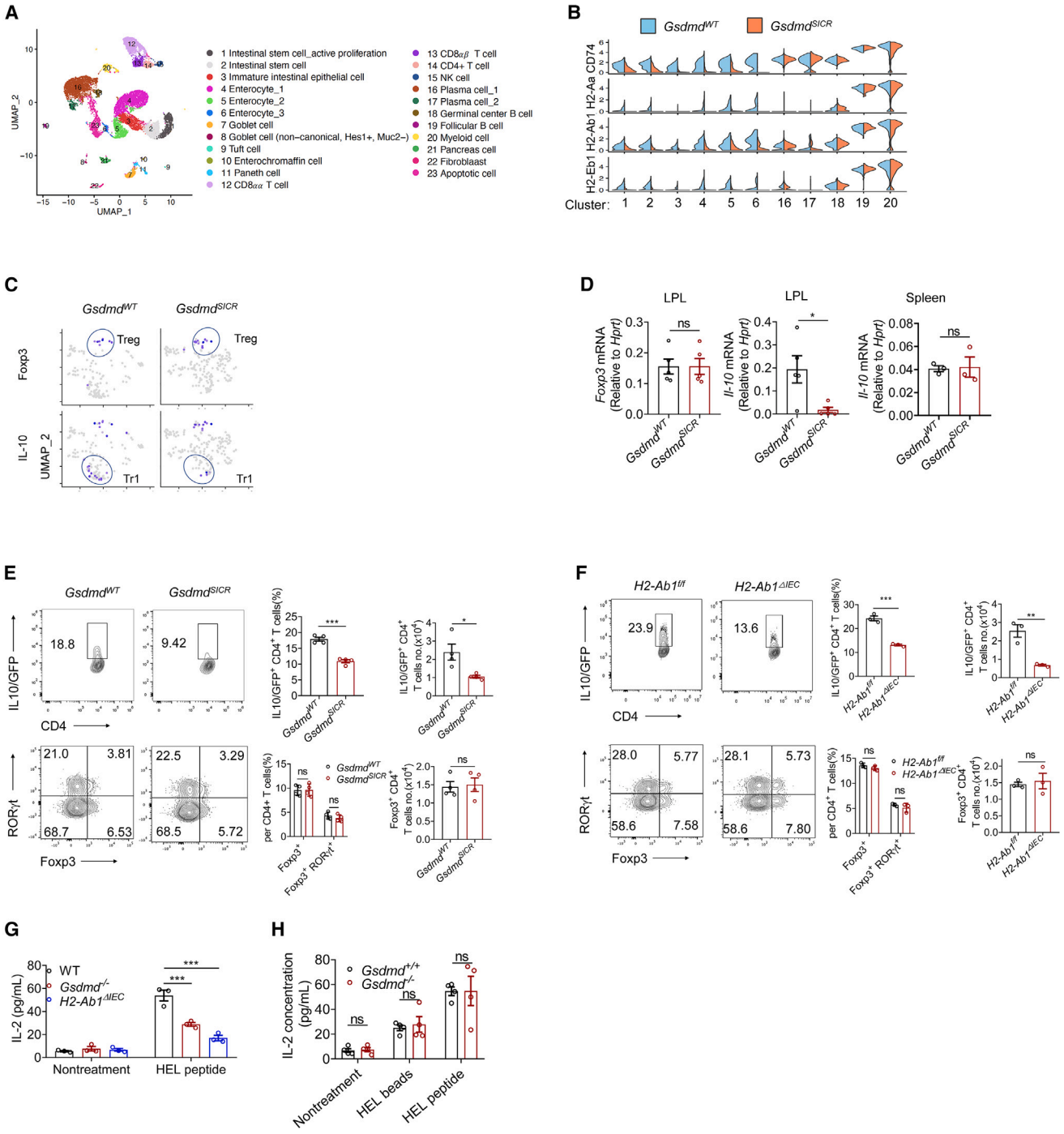


**Figure 4. The nuclear-localized GSDMD fragment regulates MHCII in IECs to induce Tr1 cells**

(A–C) Single-cell RNA sequencing (scRNA-seq) of IECs from *Gsdmd*$^{SICR}$ mutant mice compared with WT littermates. Uniform manifold approximation and projection (UMAP) plot of different cell populations from upper small intestine grouped in 23 clusters (A). Expression levels of MHCII genes in the indicated IEC clusters and typical antigen-presenting cells (APCs) clusters (B). The gene expression pattern of *Foxp3* and *IL-10* showing the populations of Treg (CD4$^+$Foxp3$^+$IL10$^+$) and Tr1 (CD4$^+$Foxp3$^-$IL10$^+$) cells from scRNA-seq (C).

(D) qPCR analysis of *IL-10* and *Foxp3* transcripts in sorted LPL CD4$^+$ T cells of upper small intestine and spleen from *Gsdmd*$^{SICR}$ mice or littermate WT mice.

(E and F) Suppressive T helper cells in the duodenum of *Gsdmd*$^{SICR}$ mice or *H2-Ab1*$^{\Delta IEC}$ mice crossed with il10-GFP mice.

(G and H) Hen egg lyzome (HEL) antigen presenting assay to investigate production of IL-2 by T cell hybridoma BO4 cells, which specifically recognize the HEL peptide presented by IECs (G) or DCs (H) from indicated mouse strains.

*(legend continued on next page)*

S3L). We observed significantly reduced expression of MHCII molecules and CIITA in small intestine IECs but not in large intestine IECs isolated from *Gsdmd*$^{-/-}$ mice or *Gsdmd*$^{\Delta IEC}$ mice compared with their WT littermates (Figures 3H–3J), which is in accord with our finding that the GSDMD-$N_{13}$ does not occur in large intestine IECs (Figure 2D). We also tested whether the GSDMD-$N_{13}$ is required for the observed differential expression levels of MHCII molecules and *Ciita* transcripts in upper small intestine IECs, and we found decreased levels of MHCII molecules/*Ciita* transcripts in upper small intestine IECs upon the following: (1) replacing normal chow with the aforementioned AA diet (Figures 3H and 3K), (2) treating mice with aforementioned CASP-3/7 inhibitor Ac-DVED-CHO (to inhibit 13/42 GSDMD cleavage) (Figures 3H and 3L), and (3) examining *Gsdmd*$^{SICR}$ mice in which there is no 13/42 GSDMD cleavage (Figures 3H and 3M). Further, qPCR analysis showed that ectopic expression of GSDMD-$N_{13}$ in colon epithelial MC38 cells caused increased levels of *Ciita* mRNA and of CIITA-targeted MHCII transcripts (Figures 3N and S3M). Notably, oral administration of protein antigens such as OVA—the major protein constituent of chicken egg whites, or bovine serum albumin (BSA), the major serum protein constituent from cows, rescue AA diet treatment—inhibited GSDMD 13/42 cleavage, as well as MHCII induction in IECs (Figures 3H and S3N). These results suggest that the presence of proteinaceous dietary antigens can promote nuclear GSDMD-$N_{13}$-mediated induction of *Ciita* in IECs, after which CIITA can induce the transcription of MHCII molecules.

By using the aforementioned purified recombinant MBP-tagged GSDMD-$N_{13}$ truncation protein, we performed IP/MS to identify potential interaction partner proteins that may involve in the transcriptional machinery of the *Ciita*/MHCII promoters. Interestingly, we found that STAT1, a known transcriptional factor that binds to *Ciita* promoter,[37] was one of the top candidates from the list of putative GSDMD-$N_{13}$-binding partners (Figures 3O and S2A; Table S1). We also found RFX5, a known transcriptional factor that binds to the promoters of genes encode MHCII molecules,[38] at relative low coverage and confidence (Figures 3O and S2A; Table S1). We confirmed the interaction between STAT1 and GSDMD-$N_{13}$ by coIP (Figures 3P and S3O); however, we found that there is no interaction between RFX5 and GSDMD-$N_{13}$ by coIP (Figure S3P). These data suggest that GSDMD-$N_{13}$ might interact with STAT1 to induce *Ciita*/MHCII molecules.

We next investigated whether GSDMD-$N_{13}$ is involved in STAT1-mediated *Ciita* transcription. For context, previous studies have demonstrated that *Ciita* expression is controlled by at least four different promoters (pI to pIV) with differential usages among different cell populations[39]: cells of myeloid origin (e.g., conventional DCs and macrophages) use pI for constitutive and IFN$\gamma$-induced *Ciita* expression, *Ciita* is driven by pIII in cells of lymphoid origin (B cells, T cells, and pDCs), and pIV is indispensable for IFN-$\gamma$-activated *Ciita* expression in non-conventional APCs such as epithelial cells.[39] We performed chromatin immunoprecipitation (ChIP) with an anti-FLAG antibody followed by qPCR in HEK293T cells transduced with the aforementioned FLAG-tagged GSDMD truncation variants. GSDMD-$N_{13}$, but not GSDMD-$C_{42}$ or full-length GSDMD, bound to the pIV promoter of *Ciita* (Figures 3Q and S3Q). We next performed ChIP with an anti-STAT1 antibody followed by qPCR in HEK293T cells transduced with GSDMD-$N_{13}$ and found that GSDMD-$N_{13}$ significantly promote the binding of STAT1 to the pIV promoter of *Ciita* (Figure 3R). We also performed ChIP with an anti-STAT1 antibody in IECs isolated from *Gsdmd*$^{\Delta IEC}$ mice, *Gsdmd*$^{SICR}$ mice, or their corresponding WT littermate controls. The qPCR results showed that the binding of STAT1 to the pIV promoter of *Ciita* was significantly diminished in IECs isolated from *Gsdmd*$^{\Delta IEC}$ mice or *Gsdmd*$^{SICR}$ mice, in comparison with that from their corresponding WT littermate controls (Figures 3S and 3T). We also validated that the expression levels of MHCII molecules and *Ciita* transcripts are diminished in IECs from *Stat1*$^{-/-}$ mice as compared with the WT mice (Figure S3R). These results support that GSDMD-$N_{13}$ interacts with STAT1 in the nucleus and together induce *Ciita* transcription, which ultimately promotes the expression of genes encode MHCII molecules.

## The nuclear-localized GSDMD fragment regulates MHCII in IECs to induce Tr1 cells

Although it is well established that antigen presentation by MHCII molecules in DC is critical in shaping the immune tolerance environment in the intestine,[40,41] antigen presentation by IECs has also been reported to induce tolerogenic immune cell populations.[8,9,11,42] Thus, we conducted single-cell RNA sequencing (scRNA-seq) to analyze both stroma and immune cell populations in *Gsdmd*$^{SICR}$ mice and the corresponding littermate controls. Unsupervised clustering of upper small intestine cells revealed 23 distinct clusters based on their specific gene expression profiles (Figures 4A and S4A). The expression of *Epcam* (which encodes EpCAM) and *Ptprc* (which encodes CD45), respectively, indicated epithelial and immune cells and the WT IECs showed enriched expression of *Gsdmd* (highest expression in Cluster4 and 5), notably, *Casp3* and *Casp7* transcripts were also enriched in these two clusters (Figure S4B). We also detected a substantial decrease in MHCII molecules expression in several cell clusters (e.g., enterocytes and intestinal stem cells [ISCs]) from *Gsdmd*$^{SICR}$ mice in comparison with their WT littermate mice (Figure 4B) and noted that MHCII molecules were barely expressed in specialized IECs such as goblet cells, paneth cells, tuft cells, and enterochromaffin cells (Figure S4C). Importantly—and providing further support for a functional association between GSDMD-$N_{13}$ and MHCII expression—no changes in MHCII molecule expression were detected between the mutant genotypes and WT littermates in typical antigen-presenting cell types that express high levels of MHCII molecules (e.g., B cells, macrophages, or DCs) in steady states (Figure 4B), which is confirmed by FACS staining of MHCII in CD103$^{+}$DCs of small intestines or in bone-marrow-derived DCs (BMDCs) from GSDMD KO mice or WT littermate mice (Figures S4D–S4F), consistent with our data showing a lack of any detected 13/42 cleavage in BMDCs in steady state (Figure S4G). These results

In (D–H), data are presented as the mean ± SEM. For comparisons between two groups, Student's t tests were used; for more than two groups, analysis of variance (ANOVA) was used; ns, not significant, *p < 0.05, **p < 0.01, ***p < 0.001, and ****p < 0.0001. (D)–(H) are representative of at least three experiments. See also Figure S4.

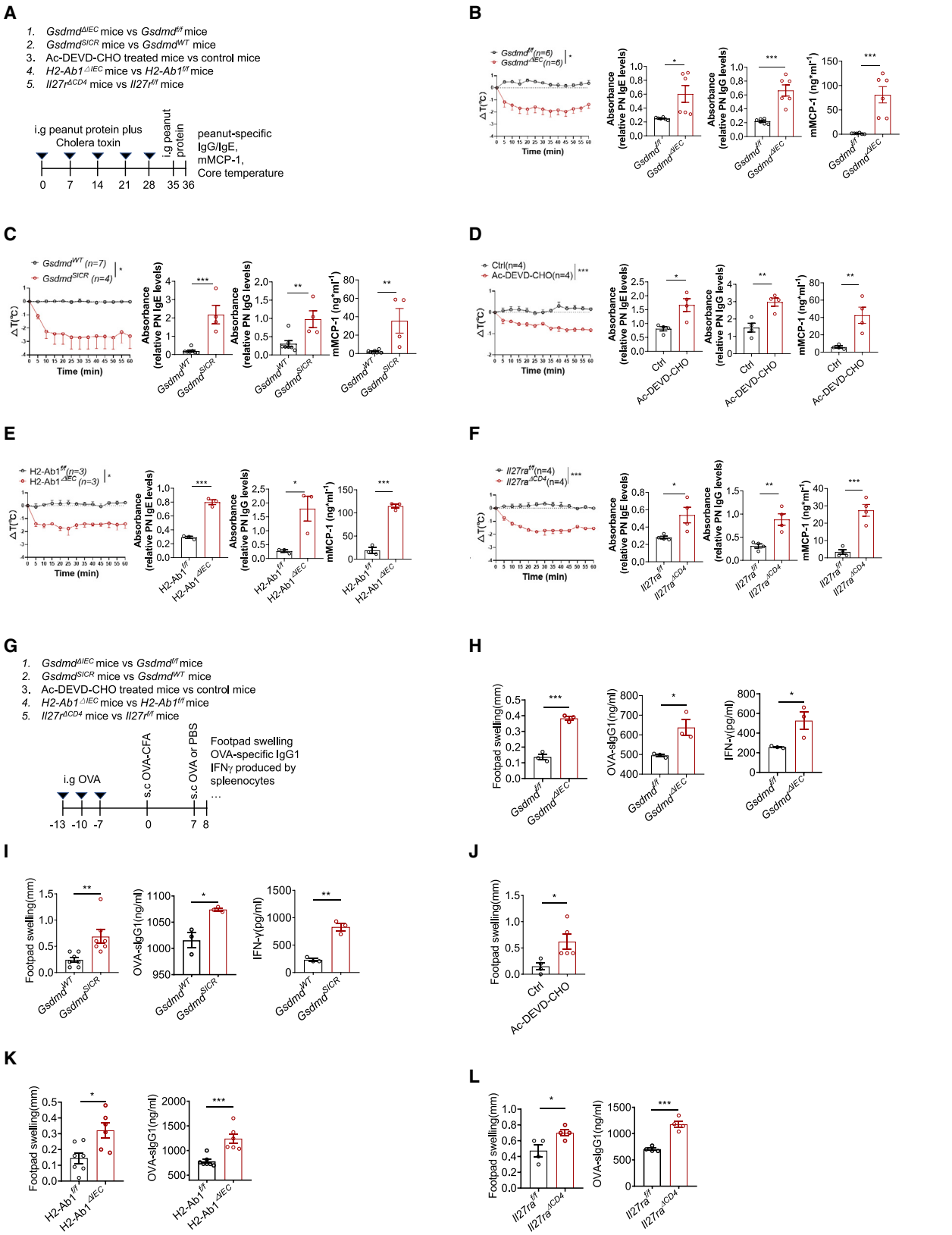


(legend on next page)

from scRNA-seq further confirmed that GSDMD-$N_{13}$ specifically regulate the expression levels of MHCII molecules in steady-state IECs but not myeloid cells.

We also explored potential functional consequences of GSDMD-$N_{13}$-induced MHCII expression in IECs. Of note, recent studies reported defects on intestinal $CD4^+$ T cells or $CD4^+IL\text{-}10^+$ regulatory T cells in mice with MHCII-deficiency in IECs.[6,8,43] Our aforementioned scRNA-seq data showed that *Gsdmd*$^{SICR}$ mice had normal immune cell signatures for major cell populations (e.g., T cells, B cell, NK cells, macrophages, DCs) compared with their WT littermates (Figure S4H). However, we observed that the inactivation of GSDMD 13/42 cleavage caused a profound reduction in Tr1 cells ($CD4^+IL\text{-}10^+Foxp3^-$) but not Treg cells ($CD4^+Foxp3^+$) in the upper small intestine (Figure 4C). In consistency, a previous study showing that the majority of IL-10 producing cells in the small intestine are Tr1 cells, whereas the majority of IL-10 producing cells in the colon are Treg cells.[44] A qPCR analysis showed that compared with WT littermates, *Il-10* expression was significantly reduced in sorted $CD4^+$ T cells from lamina propria lymphocytes (LPLs) in the upper small intestine of *Gsdmd*$^{SICR}$ mice, in comparison with that from WT littermate controls (Figure 4D); no reduction in *Il-10* expression was detected in sorted $CD4^+$ T cells from spleen of *Gsdmd*$^{SICR}$ mice, in comparison with that from WT littermate controls (Figure 3Y). Since the cellular IL-10 protein levels cannot be assessed by intracellular FACS staining in the small intestine in steady state,[45] we crossed IL-10-GFP reporter mice with *Gsdmd*$^{SICR}$ mice or with *H2-Ab1*$^{\Delta IEC}$ mice. We then isolated the LPLs from the duodenum of the resulting progeny: both the numbers and the percetages of $CD4^+IL\text{-}10\text{-}GFP^+$ cells were significantly reduced in both *Gsdmd*$^{SICR}$ mice and *H2-Ab1*$^{\Delta}$*IEC* mice compared with their corresponding WT littermates (Figures 4E and 4F). The $CD4^+Foxp3^+$ and $CD4^+Foxp3^+Ror\gamma t^+$ cell populations were not affected by the loss of GSDMD-$N_{13}$ or MHCII molecules in IECs (Figures 4E and 4F). These results suggest that GSDMD-$N_{13}$-MHCII axis in IECs supports the Tr1 population in upper small intestine.

Previous studies have reported *in vivo* that subsets of IECs that express MHCII molecules can function as unconventional antigen-presenting cells, which shape T cell populations in the intestine.[6,8,43] Moreover, in *in vitro* systems, IECs have also been previously shown to present antigens and interact with T cells.[8,9,43,46] We hypothesized that among IECs, the interaction with T cells needs the help of MHCII, which could be affected by GSDMD. We used an *in vitro* antigen presentation experimental system to determine whether IECs can efficiently present an antigen (hen egg lysozyme, HEL) to antigen-specific T cells. Specifically, we assayed MHC class II presentation in IECs and in DCs from GSDMD KO or WT littermate mice by measuring the H2-$A^b$/$HEL_{74–88}$ complex-induced secretion of IL-2 by T cell hybridoma BO4 cells. GSDMD KO in IECs resulted in significantly reduced HEL-peptide induced T cell activation; this outcome was also detected for control *H2-Ab*-deficient IECs (Figure 4G). In contrast, we found no difference in MHC class II-antigen presentation to T cells between GSDMD KO and WT DCs (Figure 4H). Together, these results demonstrate that proteinaceous dietary antigens induce nuclear GSDMD-$N_{13}$-regulated MHCII expression in IECs to support Tr1 cells in the upper small intestine.

## Inactivation of food-induced GSDMD cleavage in IECs disrupts immune tolerance to food

In light of our observations that dietary antigens sustain the 13/42 cleavage of GSDMD and that GSDMD-$N_{13}$ regulates MHCII molecules in IECs to support Tr1 cells in the upper small intestine, and considering that dietary antigens is known to induce tolerance that avoids unnecessary immune activation against essential food materials, we reasoned that 13/42 GSDMD cleavage in IECs might be involved in proteinaceous dietary-antigen-induced tolerance in the small intestine. We therefore induced an experimental food allergy model with peanut extracts in the following mice: (1) *Gsdmd*$^{\Delta IEC}$ mice versus *Gsdmd*$^{f/f}$ mice (i.e., with depletion of GSDMD from IECs), (2) *Gsdmd*$^{SICR}$ mice versus *Gsdmd*$^{WT}$ mice (blocked 13/42 cleavage of GSDMD), (3) WT mice treated with the CASP3/7 inhibitor Ac-DEVD-CHO or vehicle versus control mice (CASP3/7 inhibition), (4) *H2-Ab1*$^{\triangle IEC}$ mice versus *H2-Ab1*$^{f/f}$ mice (depletion of MHCII in IECs), and (5) because IL-27 is required for the differentiation of Tr1 cells,[47,48] the $CD4^+$ T-cell-specific knockout of *Wsx1* (subunit of the IL-27R complex) results in the depletion of Tr1 cells (Figures S5A and S5B)[47,48]; thus, we also induced the food allergy model in *Il27ra*$^{\Delta CD4}$ mice versus WT control mice (Figure 5A).

Upon exposure of mice to peanut protein extracts (PN) and cholera toxin (CT), and re-challenging these mice with PN (Figure 5A), we observed the following changes in all of the aforementioned comparisons (*Gsdmd*$^{\Delta IEC}$ mice, *Gsdmd*$^{SICR}$, *H2-Ab1*$^{\Delta IEC}$, *Il27ra*$^{\Delta CD4}$ mice, and Ac-DEVD-CHO-treated mice, compared with their respective controls): significantly increased levels of PN-specific IgE and IgG, significantly increased levels of serum mMCP-1 (mouse mast cell protease-1, a mast cell protease released upon allergen-dependent cross-linking of IgE[49]), and significantly reduced core body temperature (Figures 5B–5F). These changes are all characteristic of an anaphylactic response, and support those mice lacking GSDMD-$N_{13}$, mice lacking MHCII

**Figure 5. GSDMD KO or the cleavage-resistant GSDMD variant in IECs disrupts immune tolerance to food**

(A–F) Peanut allergy model was induced in mice from 5 comparisons (A): *Gsdmd*$^{\Delta IEC}$ mice (B), *Gsdmd*$^{SICR}$ mutant mice (C), Ac-DEVD-CHO-treated mice (D), *H2-Ab1*$^{\Delta IEC}$ mice (E), *Il27ra*$^{\Delta CD4}$ mice (F), and their corresponding WT control mice. Change in core body temperature was recorded every 5 min for 1 h after the second challenge of the mice with peanut extracts; serum peanut-specific IgE and IgG, and serum mMCP-1 were measured by ELISA.

(G–L) delayed type hypersensitivity (DTH) model was induced in mice from 5 comparisons (G): *Gsdmd*$^{\Delta IEC}$ mice (H), *Gsdmd*$^{SICR}$ mutant mice (I), or Ac-DEVD-CHO-treated mice (J), *H2-Ab1*$^{\Delta IEC}$ mice (K), *Il27ra*$^{\Delta CD4}$ mice (L), and their corresponding WT control mice. Footpad swelling was recorded after the re-challenge of the mice with OVA (H–L), serum OVA-specific IgG1 was measured by ELISA (H–K), IFN$\gamma$ production by splenocytes re-stimulated with OVA *in vitro* was measured by CBA FACS array kit (BD Biosciences) (H&I).

(B–F) and (H–L) data are presented as the mean ± SEM, for comparisons between two groups, Student's t tests were used. For body temperature curves, two-way ANOVA tests were used. *$p < 0.05$, **$p < 0.01$, ***$p < 0.001$, and ****$p < 0.0001$. (B–E) and (H–K) are representative of at least three experiments.
See also Figure S5.

in IECs, and mice lacking Tr1 cells have increased susceptibility to the food allergies. Notably, in comparison with the corresponding WT control mice, *Gsdmd*$^{\Delta IEC}$ mice, *Gsdmd*$^{SICR}$, *H2-Ab1*$^{\Delta IEC}$, and Ac-DEVD-CHO-treated mice still showed significance reduction of IEC-MHCII levels as steady states, upon challenging with PN (Figure S5C); however, *Il27ra*$^{\Delta CD4}$ mice showed no difference in IEC-MHCII level compared with the WT mice; whereas *H2-Ab1*$^{\Delta DC}$ mice showed a mild compensatory increase of IEC-MHCII level in comparison with the WT mice (Figure S5C). We also found that specific depletion of MHCII in DCs (*H2-Ab1*$^{\Delta DC}$) showed similar susceptible food allergy phenotype, compared with the littermate WT control mice (Figure S5D), indicating that antigen presentations in both DCs and IECs may complementarily contribute to the immune tolerance to food.

Consistent with our findings from the aforementioned peanut allergy model, we found that these mice had impaired establishment of immune tolerance to another food antigen when we evaluated delayed type hypersensitivity (DTH) responses to OVA (Figure 5G). Specifically, feeding OVA to WT mice or *Gsdmd*$^{\Delta DC}$ mice induced tolerance (Figures 5G and S5E), whereas feeding OVA to *Gsdmd*$^{\Delta IEC}$ mice, *Gsdmd*$^{SICR}$, and CASP3/7 inhibitor Ac-DEVD-CHO-treated mice failed to induce oral tolerance; instead, these mice showed foot swelling, higher titers of anti-OVA IgG1 in the serum, and elevated expression of IFN$\gamma$ by splenocytes (Figures 5G–5J, S5F, and S5G). Note that the same phenotypes were detected upon DTH model induction in *H2-Ab1*$^{\Delta IEC}$ and *Il27ra*$^{\Delta CD4}$ mice (Figures 5K and 5L). Collectively, these results demonstrate that the IEC-expressed GSDMD and MHCII, and Tr1 cells in the upper small intestine induce the immune tolerance to food.

## DISCUSSION

As the primary barrier between host cells and numerous microbes and dietary antigens, IECs are well positioned to regulate tolerance to food and commensals while preserving immunity against pathogens. GSDMD is highly expressed in IECs, although the functional consequences of this expression, especially in upper small intestine where there is full of food antigen, are not understood. GSDMD is considered to be the executor of pyroptosis in myeloid cells[19,20]: its 30-kD N-terminal cleaved form has been shown to form pores that breach cell membranes.[15,32] Beyond this previously reported inflammatory role of GSDMD, this study reveals a divergent role wherein GSDMD's 13-kD N-terminal cleaved form translocates to the nucleus and functions to mediate immune tolerance to food by inducing CIITA and MHCII expression in IECs and Tr1 cells in LPL. Thus, it appears that the differential cleavage of GSDMD can be understood conceptually as a regulatory hub to control innate immunity versus food tolerance in the small intestine (graphical abstract).

Although CASP-3/7-mediated cleavage of GSDMD at D88 has been reported *in vitro*[25–29] and we also repeated that the apoptotic triggers that activate CASP-3/7 could induce the generation of GSDMD-$N_{13}$ in macrophages (Figure S5H), our work confirmed the existence of this cleavage *in vivo* and demonstrated both physiological and immune-tolerance-related functions of this cleavage. There is active debate about whether this cleavage inactivates the pyroptotic activity of GSDMD. One side holds the idea that cleavage of GSDMD at D88 inactivates its pyroptotic activity,[25,50] the other side emphasizes that GSDMD inactivation at D88 does not suppress pyroptosis or IL-1$\beta$ secretion upon canonical inflammasome activation.[26] However, this divergence could plausibly result from the influence of experimental conditions that may artificially introduce high doses of different caspase proteins *in vitro*. According to our observation, the IECs of *Gsdmd*$^{SICR}$ mutant mice showed no difference in the extent of pyroptotic cleavage of GSDMD (Figure 2M), supporting the idea that the 13/42 cleavage of GSDMD by CASP-3/7 does not affect the pyroptotic cleavage of GSDMD in small intestine. Moreover, when triggering pyroptosis in the bone marrow derived macrophages derived from *Gsdmd*$^{SICR}$ mice, the pyroptotic cleavage of GSDMD was also unaffected (Figure S2I). Noted that the IECs from *Gsdmd*$^{SICR}$ mutant mice did not affect cell death in comparison with the WT littermate mice (Figures S2H and S2J). These data exclude the possible involvement of inactivation of GSDMD-$N_{30}$-mediated pyroptosis or CASP-3/7 induced apoptosis in GSDMD-$N_{13}$-induced regulation of IECs' MHCII expression. STAT1 was reported to regulate *Ciita* function and MHCII expression in non-hematopoietic cells and our work further support this regulation in IECs (Figure S3R). We also found that GSDMD-$N_{13}$ could translocate into nucleus of IECs and enhance STAT1 function in promoting *Ciita* expression (Figures 3P–3T), as well as other STAT1-targeted genes[51] (Figure S5I).

We and others showed that the intestinal microbiota is required for the MHCII expression in IECs from ileum or distal jejunum[6,8] (Figures S5J–S5L); however, in IECs from duodenum, MHCII expression is largely rely on the dietary antigens (Figures S5J–S5L). In consistent with that, GSDMD deficiency in IEC but not antibiotics treatment led to the reduction of the IEC-MHCII levels in duodenum, whereas antibiotics treatment but not GSDMD deficiency in IEC led to the reduction of the IEC-MHCII levels in ileum from mice challenged with peanut allergen (Figure S5M). Furthermore, in the duodenum of IL-10-GFP/Foxp3-RFP double reporter mice, treatment with AAD or Ac-DEVD-CHO but not antibiotics led to the reduction of Tr1 cells (IL-10-GFP$^+$ Foxp3-RFP$^-$) (Figures S5N and S5O). When we deplete the microbiota by antibiotics treatment before performing the peanut allergy model in *Gsdmd*$^{\Delta IEC}$ mice and littermate control mice, we found significantly increased levels of PN-specific IgE and IgG; significantly increased levels of serum mMCP-1, and significantly reduced core body temperature in *Gsdmd*$^{\Delta IEC}$ mice (Figure S5P), showing that these mice are more susceptible to the food allergies even without microbiota. These results suggest that food antigens and microbiota corporately regulate the MHCII levels in IECs from different intestinal segments.

There is increasing interests in atypical MHCII functions. Although small intestine IECs are known to constitutively express MHCII molecules, the capacity of these cells to process and present antigens is controversial. Our *in vitro* culture system with the HEL antigen supports the antigen-presenting ability of IECs to T cells (Figures 4G and 4H). Studies have also reported roles for IECs-expressed MHCII molecules in shaping CD4 T cell populations in the intestine.[6–8,43] Lack of MHCII expression on ISCs has been shown to reduce the number of CD4$^+$ T cells in

the vicinity,[43] and increased IEC MHC class II expression results in increased proliferation of $CD4^+$ T cells after BMT in the lower small intestine.[6] Also, a recent study showed that genetic loss of MHCII in IECs results in reduction of the Tr1 cell population.[8] In agreement with Tuganbaev et al.,[8] we found a significant decrease in Tr1 cells in the duodenum of $Gsdmd^{SICR}$ mice and $H2\text{-}Ab1^{\Delta IEC}$ mice compared with their WT littermates (Figures 4E and 4F). These studies support the idea that GSDMD regulated MHCII molecules expression in IECs support the T cell populations in the upper small intestine. Notably, the general lack of the expression of co-stimulatory molecules, such as CD80, CD86, and CD40, and the relative high expression of co-inhibitory molecules, such as PD-L1, in IECs from upper small intestine might be the potential reason for the preferential regulation of immunosuppressive T cell responses by IEC-MHCII in upper small intestine (Figure S5Q).

In summary, we discovered that IECs accumulate a non-canonical cleaved form of GSDMD in response to proteinaceous dietary antigens, thereby supporting the regulatory T helper subset Tr1 cells through IEC-mediated antigen presentation, and consequently inducing the immune tolerance to food. These insights concerning GSDMD's divergent roles in immunity versus tolerance deepen our understanding of innate immunity generally and may facilitate the development of therapies to treat food allergies.

### Limitations of the study

This study provides insights about how a non-canonical cleavage form of GSDMD is induced by food antigens in IECs to maintain immune tolerance to food. However, it is still unclear the exact kind of peptide(s) that is responsible to induce the tolerance. Is there any length preference or sequence preference to activate CASP-3 and CASP-7? What is the molecular architecture of the GSDMD-$N_{13}$/STAT1 transcriptional machinery? Are there any antigen preferences presented by MHCII molecules in IECs and/or DCs? Given that Treg cells and Tr1 cells are regionally distributed along the intestinal tract, how do they cooperate to maintain tolerance to commensals, foods, and perhaps other environmental cues? Whether and how do MHCII-expressing APCs, such as DCs, ILC3s, and IECs, cooperate to sense and induce tolerances to commensals, foods, and other environmental cues? We expect that examination of these questions in the future will not only provide more details and depth to understand the role of GSDMD in IECs and the mechanism for the induction of food tolerance but also open therapeutic opportunities for food allergies.

## STAR★METHODS

Detailed methods are provided in the online version of this paper and include the following:



### SUPPLEMENTAL INFORMATION

Supplemental information can be found online at https://doi.org/10.1016/j.cell.2023.05.027.

### ACKNOWLEDGMENTS

We thank Dr. Peter Cresswell for providing the hen egg lysosyme antigen presentation assay.[52] We thank Dr. Feng Shao for providing GSDMD floxed mice. We thank Dr. Zhinan Yin for providing Il27ra floxed mice. We thank Dr. Anthony Rongvaux and Dr. Stephanie Eisenbarth for helpful discussion. We thank Baifa Sheng for maintaining some of the mouse colonies. We thank Shengdan Bai and Xuequn Chen for plasmids construction. We thank Guorong Zhang and Anming Wang for assistance with the AVC treatment experiments. We thank Sicheng Fu for help with DTH animal experiments. We thank Huabin He for preparing the GSDMD floxed mice. This work was supported by grants from the National Key R&D Program of China (2018YFA0508000) (to S.Z.), the Strategic Priority Research Program of the Chinese Academy of Sciences (XDB290 30101) (to S.Z.), the CAS Project for Young Scientists in Basic Research (YSBR-074); and the National Natural Science Foundation of China (82061148013, 81822021, and 81821001) (to S.Z.). R.A.F. is an investigator of the Howard Hughes Medical Institute.

### AUTHOR CONTRIBUTIONS

K.H., T.W., and D.W. designed, performed, and interpreted experiments. J.H. helped with animal experiments. T.Z. and W.T. analyzed the RNA-seq and scRNA-seq data. Z.W. and Q.L. performed the HEL antigen presentation assay. R.Z. and Z.T. provided critical comments and suggestions. S.Z. and R.A.F. supervised the project. S.Z. wrote the manuscript.

## DECLARATION OF INTERESTS

S.Z. is a cofounder of Ibiome which studies microbial regulation of immune responses. R.A.F. is a cofounder of Ventus, which studies inflammatory pathways. Both in topics unrelated to the subject of this work.

Received: September 21, 2021
Revised: March 3, 2023
Accepted: May 17, 2023
Published: June 15, 2023

## REFERENCES

1. Grigg, J.B., Shanmugavadivu, A., Regen, T., Parkhurst, C.N., Ahmed, A., Joseph, A.M., Mazzucco, M., Gronke, K., Diefenbach, A., Eberl, G., et al. (2021). Antigen-presenting innate lymphoid cells orchestrate neuroinflammation. Nature *600*, 707–712. https://doi.org/10.1038/s41586-021-04136-4.
2. Hepworth, M.R., Monticelli, L.A., Fung, T.C., Ziegler, C.G., Grunberg, S., Sinha, R., Mantegazza, A.R., Ma, H.L., Crawford, A., Angelosanto, J.M., et al. (2013). Innate lymphoid cells regulate CD4+ T-cell responses to intestinal commensal bacteria. Nature *498*, 113–117. https://doi.org/10.1038/nature12240.
3. Lyu, M., Suzuki, H., Kang, L., Gaspal, F., Zhou, W., Goc, J., Zhou, L., Zhou, J., Zhang, W., et al.; JRI Live Cell Bank (2022). ILC3s select microbiota-specific regulatory T cells to establish tolerance in the gut. Nature *610*, 744–751. https://doi.org/10.1038/s41586-022-05141-x.
4. Kim, K.S., Hong, S.W., Han, D., Yi, J., Jung, J., Yang, B.G., Lee, J.Y., Lee, M.J., and Surh, C.D. (2016). Dietary antigens limit mucosal immunity by inducing regulatory T cells in the small intestine. Science *351*, 858–863. https://doi.org/10.1126/science.aac5560.
5. Hong, S.W., Krueger, P.D., Osum, K.C., Dileepan, T., Herman, A., Mueller, D.L., and Jenkins, M.K. (2022). Immune tolerance of food is mediated by layers of $CD4^+$ T cell dysfunction. Nature *607*, 762–768. https://doi.org/10.1038/s41586-022-04916-6.
6. Koyama, M., Mukhopadhyay, P., Schuster, I.S., Henden, A.S., Hülsdünker, J., Varelias, A., Vetizou, M., Kuns, R.D., Robb, R.J., Zhang, P., et al. (2019). MHC Class II antigen presentation by the intestinal epithelium initiates graft-versus-host disease and is influenced by the microbiota. Immunity *51*, 885–898.e7. https://doi.org/10.1016/j.immuni.2019.08.011.
7. Moon, S., Park, Y., Hyeon, S., Kim, Y.-M., Kim, J.-H., Kim, H., Park, S., Lee, K.-J., Koo, B.-K., Ha, S.-J., and Lee, S.-W. (2021). Niche-specific MHC II and PD-L1 regulate CD4+CD8αα+ intraepithelial lymphocyte differentiation. J. Exp. Med. *218*, e20201665. https://doi.org/10.1084/jem.20201665.
8. Tuganbaev, T., Mor, U., Bashiardes, S., Liwinski, T., Nobs, S.P., Leshem, A., Dori-Bachash, M., Thaiss, C.A., Pinker, E.Y., Ratiner, K., et al. (2020). Diet diurnally regulates small intestinal microbiome-epithelial-immune homeostasis and enteritis. Cell *182*, 1441–1459.e21. https://doi.org/10.1016/j.cell.2020.08.027.
9. Westendorf, A.M., Fleissner, D., Groebe, L., Jung, S., Gruber, A.D., Hansen, W., and Buer, J. (2009). CD4+Foxp3+ regulatory T cell expansion induced by antigen-driven interaction with intestinal epithelial cells independent of local dendritic cells. Gut *58*, 211–219. https://doi.org/10.1136/gut.2008.151720.
10. Westendorf, A.M., Bruder, D., Hansen, W., and Buer, J. (2006). Intestinal epithelial antigen induces CD4+ T cells with regulatory phenotype in a transgenic autoimmune mouse model. Ann. NY Acad. Sci. *1072*, 401–406. https://doi.org/10.1196/annals.1326.035.
11. Cruickshank, S.M., McVay, L.D., Baumgart, D.C., Felsburg, P.J., and Carding, S.R. (2004). Colonic epithelial cell mediated suppression of CD4 T cell activation. Gut *53*, 678–684. https://doi.org/10.1136/gut.2003.029967.
12. He, W.T., Wan, H., Hu, L., Chen, P., Wang, X., Huang, Z., Yang, Z.H., Zhong, C.Q., and Han, J. (2015). Gasdermin D is an executor of pyroptosis and required for interleukin-1beta secretion. Cell Res. *25*, 1285–1298. https://doi.org/10.1038/cr.2015.139.
13. Kayagaki, N., Stowe, I.B., Lee, B.L., O'Rourke, K., Anderson, K., Warming, S., Cuellar, T., Haley, B., Roose-Girma, M., Phung, Q.T., et al. (2015). Caspase-11 cleaves gasdermin D for non-canonical inflammasome signalling. Nature *526*, 666–671. https://doi.org/10.1038/nature15541.
14. Shi, J., Zhao, Y., Wang, K., Shi, X., Wang, Y., Huang, H., Zhuang, Y., Cai, T., Wang, F., and Shao, F. (2015). Cleavage of GSDMD by inflammatory caspases determines pyroptotic cell death. Nature *526*, 660–665. https://doi.org/10.1038/nature15514.
15. Liu, X., Zhang, Z., Ruan, J., Pan, Y., Magupalli, V.G., Wu, H., and Lieberman, J. (2016). Inflammasome-activated gasdermin D causes pyroptosis by forming membrane pores. Nature *535*, 153–158. https://doi.org/10.1038/nature18629.
16. Humphries, F., Shmuel-Galia, L., Ketelut-Carneiro, N., Li, S., Wang, B., Nemmara, V.V., Wilson, R., Jiang, Z., Khalighinejad, F., Muneeruddin, K., et al. (2020). Succination inactivates gasdermin D and blocks pyroptosis. Science *369*, 1633–1637. https://doi.org/10.1126/science.abb9818.
17. Orning, P., Weng, D., Starheim, K., Ratner, D., Best, Z., Lee, B., Brooks, A., Xia, S., Wu, H., Kelliher, M.A., et al. (2018). Pathogen blockade of TAK1 triggers caspase-8-dependent cleavage of gasdermin D and cell death. Science *362*, 1064–1069. https://doi.org/10.1126/science.aau2818.
18. Rühl, S., Shkarina, K., Demarco, B., Heilig, R., Santos, J.C., and Broz, P. (2018). ESCRT-dependent membrane repair negatively regulates pyroptosis downstream of GSDMD activation. Science *362*, 956–960. https://doi.org/10.1126/science.aar7607.
19. Hu, B., Jin, C.C., Li, H.B., Tong, J.Y., Ouyang, X.S., Cetinbas, N.M., Zhu, S., Strowig, T., Lam, F.C., Zhao, C., et al. (2016). The DNA-sensing AIM2 inflammasome controls radiation-induced cell death and tissue injury. Science *354*, 765–768. https://doi.org/10.1126/science.aaf7532.
20. Zhu, S., Ding, S.Y., Wang, P.H., Wei, Z., Pan, W., Palm, N.W., Yang, Y., Yu, H., Li, H.B., Wang, G., et al. (2017). Nlrp9b inflammasome restricts rotavirus infection in intestinal epithelial cells. Nature *546*, 667–670. https://doi.org/10.1038/nature22967.
21. Schwarzer, R., Jiao, H., Wachsmuth, L., Tresch, A., and Pasparakis, M. (2020). FADD and caspase-8 regulate gut homeostasis and inflammation by controlling MLKL- and GSDMD-mediated death of intestinal epithelial cells. Immunity *52*, 978–993.e6. https://doi.org/10.1016/j.immuni.2020.04.002.
22. Bulek, K., Zhao, J., Liao, Y., Rana, N., Corridoni, D., Antanaviciute, A., Chen, X., Wang, H., Qian, W., Miller-Little, W.A., et al. (2020). Epithelial-derived gasdermin D mediates nonlytic IL-1beta release during experimental colitis. J. Clin. Invest. *130*, 4218–4234. https://doi.org/10.1172/JCI138103.
23. Zhao, Y., Yang, J., Shi, J., Gong, Y.N., Lu, Q., Xu, H., Liu, L., and Shao, F. (2011). The NLRC4 inflammasome receptors for bacterial flagellin and type III secretion apparatus. Nature *477*, 596–600. https://doi.org/10.1038/nature10510.
24. Guo, C.S., Xie, S.J., Chi, Z.X., Zhang, J.H., Liu, Y.Y., Zhang, L., Zheng, M.Z., Zhang, X., Xia, D.J., Ke, Y.H., et al. (2016). Bile acids control inflammation and metabolic disorder through inhibition of NLRP3 inflammasome. Immunity *45*, 802–816. https://doi.org/10.1016/j.immuni.2016.09.008.
25. Taabazuing, C.Y., Okondo, M.C., and Bachovchin, D.A. (2017). Pyroptosis and apoptosis pathways engage in bidirectional crosstalk in monocytes and macrophages. Cell Chem. Biol. *24*, 507–514.e4. https://doi.org/10.1016/j.chembiol.2017.03.009.
26. Demarco, B., Grayczyk, J.P., Bjanes, E., Le Roy, D., Tonnus, W., Assenmacher, C.-A., Radaelli, E., Fettrelet, T., Mack, V., Linkermann, A., et al. (2020). Caspase-8–dependent gasdermin D cleavage promotes antimicrobial defense but confers susceptibility to TNF-induced lethality. Sci. Adv. *6*.

27. Chen, K.W., Demarco, B., Heilig, R., Shkarina, K., Boettcher, A., Farady, C.J., Pelczar, P., and Broz, P. (2019). Extrinsic and intrinsic apoptosis activate pannexin-1 to drive NLRP3 inflammasome assembly. EMBO J. *38*. https://doi.org/10.15252/embj.2019101638.

28. Orning, P., Weng, D., Starheim, K., Ratner, D., Best, Z., Lee, B., Alexandria, B., Xia, S., Wu, H., and Kelliher, M.A. (2018). Pathogen blockade of TAK1 triggers caspase-8-dependent cleavage of gasdermin D and cell death. Science *362*, 1064–1069.

29. Sarhan, J., Liu, B.C., Muendlein, H.I., Li, P., Nilson, R., Tang, A.Y., Rongvaux, A., Bunnell, S.C., Shao, F., Green, D.R., and Poltorak, A. (2018). Caspase-8 induces cleavage of gasdermin D to elicit pyroptosis during Yersinia infection. Proc. Natl. Acad. Sci. USA *115*, E10888–E10897. https://doi.org/10.1073/pnas.1809548115.

30. Rogers, C., Fernandes-Alnemri, T., Mayes, L., Alnemri, D., Cingolani, G., and Alnemri, E.S. (2017). Cleavage of DFNA5 by caspase-3 during apoptosis mediates progression to secondary necrotic/pyroptotic cell death. Nat. Commun. *8*, 14128. https://doi.org/10.1038/ncomms14128.

31. Buckley, C.D., Pilling, D., Henriquez, N.V., Parsonage, G., Threlfall, K., Scheel-Toellner, D., Simmons, D.L., Akbar, A.N., Lord, J.M., and Salmon, M. (1999). RGD peptides induce apoptosis by direct caspase-3 activation. Nature *397*, 534–539. https://doi.org/10.1038/17409.

32. Ding, J., Wang, K., Liu, W., She, Y., Sun, Q., Shi, J., Sun, H., Wang, D.C., and Shao, F. (2016). Pore-forming activity and structural autoinhibition of the gasdermin family. Nature *535*, 111–116. https://doi.org/10.1038/nature18590.

33. Lin, C.S., Liang, Y., Su, S.G., Zheng, Y.L., Yang, X., Jiang, N., Fu, L., Zhou, J., Zhang, Y., Deng, R., et al. (2022). Nucleoporin 93 mediates beta-catenin nuclear import to promote hepatocellular carcinoma progression and metastasis. Cancer Lett. *526*, 236–247. https://doi.org/10.1016/j.canlet.2021.11.001.

34. Wagstaff, K.M., and Jans, D.A. (2009). Importins and beyond: non-conventional nuclear transport mechanisms. Traffic *10*, 1188–1198. https://doi.org/10.1111/j.1600-0854.2009.00937.x.

35. Xiao, Z., Latek, R., and Lodish, H.F. (2003). An extended bipartite nuclear localization signal in Smad4 is required for its nuclear import and transcriptional activity. Oncogene *22*, 1057–1069. https://doi.org/10.1038/sj.onc.1206212.

36. Masternak, K., Muhlethaler-Mottet, A., Villard, J., Zufferey, M., Steimle, V., and Reith, W. (2000). CIITA is a transcriptional coactivator that is recruited to MHC class II promoters by multiple synergistic interactions with an enhanceosome complex. Genes Dev. *14*, 1156–1166.

37. Muhlethaler-Mottet, A., Di Berardino, W., Otten, L.A., and Mach, B. (1998). Activation of the MHC class II transactivator CIITA by interferon-gamma requires cooperative interaction between Stat1 and USF-1. Immunity *8*, 157–166.

38. Moreno, C.S., Beresford, G.W., Louis-Plence, P., Morris, A.C., and Boss, J.M. (1999). CREB regulates MHC class II expression in a CIITA-dependent manner. Immunity *10*, 143–151.

39. LeibundGut-Landmann, S., Waldburger, J.M., Krawczyk, M., Otten, L.A., Suter, T., Fontana, A., Acha-Orbea, H., and Reith, W. (2004). Mini-review: specificity and expression of CIITA, the master regulator of MHC class II genes. Eur. J. Immunol. *34*, 1513–1525. https://doi.org/10.1002/eji.200424964.

40. Matteoli, G., Mazzini, E., Iliev, I.D., Mileti, E., Fallarino, F., Puccetti, P., Chieppa, M., and Rescigno, M. (2010). Gut CD103+ dendritic cells express indoleamine 2,3-dioxygenase which influences T regulatory/T effector cell balance and oral tolerance induction. Gut *59*, 595–604. https://doi.org/10.1136/gut.2009.185108.

41. Coombes, J.L., and Maloy, K.J. (2007). Control of intestinal homeostasis by regulatory T cells and dendritic cells. Semin. Immunol. *19*, 116–126. https://doi.org/10.1016/j.smim.2007.01.001.

42. Karlsson, M., Lundin, S., Dahlgren, U., Kahu, H., Pettersson, I., and Telemo, E. (2001). "Tolerosomes" are produced by intestinal epithelial cells. Eur. J. Immunol. *31*, 2892–2900. https://doi.org/10.1002/1521-4141(2001010)31:10<2892::aid-immu2892>3.0.co;2-i.

43. Biton, M., Haber, A.L., Rogel, N., Burgin, G., Beyaz, S., Schnell, A., Ashenberg, O., Su, C.W., Smillie, C., Shekhar, K., et al. (2018). T helper cell cytokines modulate intestinal stem cell renewal and differentiation. Cell *175*, 1307–1320.e22. https://doi.org/10.1016/j.cell.2018.10.008.

44. Maynard, C.L., Harrington, L.E., Janowski, K.M., Oliver, J.R., Zindl, C.L., Rudensky, A.Y., and Weaver, C.T. (2007). Regulatory T cells expressing interleukin 10 develop from Foxp3+ and Foxp3- precursor cells in the absence of interleukin 10. Nat. Immunol. *8*, 931–941. https://doi.org/10.1038/ni1504.

45. Kim, M., Galan, C., Hill, A.A., Wu, W.J., Fehlner-Peach, H., Song, H.W., Schady, D., Bettini, M.L., Simpson, K.W., Longman, R.S., et al. (2018). Critical Role for the Microbiota in CX3CR1+ Intestinal Mononuclear Phagocyte Regulation of Intestinal T Cell Responses. Immunity *49*, 151–163.e5. https://doi.org/10.1016/j.immuni.2018.05.009.

46. Vezys, V., Olson, S., and Lefrançois, L. (2000). Expression of intestine-specific antigen reveals novel pathways of CD8 T cell tolerance induction. Immunity *12*, 505–514. https://doi.org/10.1016/s1074-7613(00)80202-2.

47. Awasthi, A., Carrier, Y., Peron, J.P.S., Bettelli, E., Kamanaka, M., Flavell, R.A., Kuchroo, V.K., Oukka, M., and Weiner, H.L. (2007). A dominant function for interleukin 27 in generating interleukin 10–producing anti-inflammatory T cells. Nat. Immunol. *8*, 1380–1389.

48. Pot, C., Apetoh, L., Awasthi, A., and Kuchroo, V.K. (2011). Induction of regulatory Tr1 cells and inhibition of T(H)17 cells by IL-27. Semin. Immunol. *23*, 438–445. https://doi.org/10.1016/j.smim.2011.08.003.

49. Platzer, B., Baker, K., Vera, M.P., Singer, K., Panduro, M., Lexmond, W.S., Turner, D., Vargas, S.O., Kinet, J.-P., Maurer, D., et al. (2015). Dendritic cell-bound IgE functions to restrain allergic inflammation at mucosal sites. Mucosal Immunol. *8*, 516–532. https://doi.org/10.1038/mi.2014.85.

50. Shi, C.S., and Kehrl, J.H. (2019). Bcl-2 regulates pyroptosis and necroptosis by targeting BH3-like domains in GSDMD and MLKL. Cell Death Discov. *5*, 151. https://doi.org/10.1038/s41420-019-0230-2.

51. Robertson, G., Hirst, M., Bainbridge, M., Bilenky, M., Zhao, Y., Zeng, T., Euskirchen, G., Bernier, B., Varhol, R., Delaney, A., et al. (2007). Genome-wide profiles of STAT1 DNA association using chromatin immunoprecipitation and massively parallel sequencing. Nat. Methods *4*, 651–657. https://doi.org/10.1038/nmeth1068.

52. van Es, J.H., Jay, P., Gregorieff, A., van Gijn, M.E., Jonkheer, S., Hatzis, P., Thiele, A., van den Born, M., Begthel, H., Brabletz, T., et al. (2005). Wnt signalling induces maturation of Paneth cells in intestinal crypts. Nat. Cell Biol. *7*, 381–386. https://doi.org/10.1038/ncb1240.

53. Stuart, T., Butler, A., Hoffman, P., Hafemeister, C., Papalexi, E., Mauck, W.M., 3rd, Hao, Y., Stoeckius, M., Smibert, P., and Satija, R. (2019). Comprehensive integration of single-cell data. Cell *177*, 1888–1902.e21. https://doi.org/10.1016/j.cell.2019.05.031.

54. Zheng, G.X., Terry, J.M., Belgrader, P., Ryvkin, P., Bent, Z.W., Wilson, R., Ziraldo, S.B., Wheeler, T.D., McDermott, G.P., Zhu, J., et al. (2017). Massively parallel digital transcriptional profiling of single cells. Nat. Commun. *8*, 14049. https://doi.org/10.1038/ncomms14049.

55. Love, M.I., Huber, W., and Anders, S. (2014). Moderated estimation of fold change and dispersion for RNA-seq data with DESeq2. Genome Biol. *15*, 550. https://doi.org/10.1186/s13059-014-0550-8.

56. Dobin, A., Davis, C.A., Schlesinger, F., Drenkow, J., Zaleski, C., Jha, S., Batut, P., Chaisson, M., and Gingeras, T.R. (2013). STAR: ultrafast universal RNA-seq aligner. Bioinformatics *29*, 15–21. https://doi.org/10.1093/bioinformatics/bts635.

57. Kosugi, S., Hasebe, M., Tomita, M., and Yanagawa, H. (2009). Systematic identification of cell cycle-dependent yeast nucleocytoplasmic shuttling proteins by prediction of composite motifs. Proc. Natl. Acad. Sci. USA *106*, 10171–10176. https://doi.org/10.1073/pnas.0900604106.

58. Nguyen Ba, A.N., Pogoutse, A., Provart, N., and Moses, A.M. (2009). NLStradamus: a simple Hidden Markov Model for nuclear localization

signal prediction. BMC Bioinformatics *10*, 202. https://doi.org/10.1186/1471-2105-10-202.

59. van Wijk, F., Nierkens, S., Hassing, I., Feijen, M., Koppelman, S.J., de Jong, G.A.H., Pieters, R., and Knippels, L.M.J. (2005). The effect of the food matrix on in vivo immune responses to purified peanut allergens. Toxicol. Sci. *86*, 333–341. https://doi.org/10.1093/toxsci/kfi187.

60. Stefka, A.T., Feehley, T., Tripathi, P., Qiu, J., McCoy, K., Mazmanian, S.K., Tjota, M.Y., Seo, G.Y., Cao, S., Theriault, B.R., et al. (2014). Commensal bacteria protect against food allergen sensitization. Proc. Natl. Acad. Sci. USA *111*, 13145–13150. https://doi.org/10.1073/pnas.1412008111.

61. Macosko, E.Z., Basu, A., Satija, R., Nemesh, J., Shekhar, K., Goldman, M., Tirosh, I., Bialas, A.R., Kamitaki, N., Martersteck, E.M., et al. (2015). Highly parallel genome-wide expression profiling of individual cells using nanoliter droplets. Cell *161*, 1202–1214. https://doi.org/10.1016/j.cell.2015.05.002.

62. Satija, R., Farrell, J.A., Gennert, D., Schier, A.F., and Regev, A. (2015). Spatial reconstruction of single-cell gene expression data. Nat. Biotechnol. *33*, 495–502. https://doi.org/10.1038/nbt.3192.

63. Butler, A., Hoffman, P., Smibert, P., Papalexi, E., and Satija, R. (2018). Integrating single-cell transcriptomic data across different conditions, technologies, and species. Nat. Biotechnol. *36*, 411–420. https://doi.org/10.1038/nbt.4096.

## STAR★METHODS

### KEY RESOURCES TABLE

| REAGENT or RESOURCE | SOURCE | IDENTIFIER |
|---|---|---|
| Antibodies | | |
| Rabbit monoclonal anti-GSDMD antibody | Abcam | Cat# ab219800; RRID: AB_2888940 |
| Rabbit monoclonal anti-GSDMD antibody | Abcam | Cat# ab209845; RRID: AB_2783550 |
| Rabbit monoclonal anti- Cleaved Gasdermin D (Asp276) (E3E3P) antibody | Cell Signaling Technology | Cat# 10137, RRID:AB_2923068 |
| Mouse monoclonal anti-Beta Actin antibody | Proteintech | Cat#: 66009-1-Ig; RRID:AB_2687938 |
| Mouse monoclonal anti-FLAG antibody | Sigma–Aldrich | Cat#: F1804; RRID: AB_262044 |
| Rabbit polyclonal anti-MYC antibody | Proteintech | Cat# 16286-1-AP, RRID:AB_11182162 |
| Mouse monoclonal anti-HA antibody | Abmart | Cat# M20003, RRID:AB_2864345 |
| Mouse anti-Caspase-1 (p20) antibody | Adipogen | Cat#: AG-20B-0042-C100; RRID: AB_2755041 |
| Rabbit monoclonal anti- Cleaved Caspase-7 (Asp198) (D6H1) antibody | Cell Signaling Technology | Cat# 8438, RRID:AB_11178377 |
| Rabbit monoclonal anti-Caspase-3 antibody | Abcam | Cat# ab184787, RRID:AB_2827742 |
| Rabbit monoclonal anti-Caspase-7 antibody | Abcam | Cat# ab181579, RRID:AB_2925166 |
| Rabbit polyclonal anti-STAT1 antibody | Cell Signaling Technology | Cat# 9172, RRID:AB_2198300 |
| Goat Anti-Mouse IgE-HRP | SouthernBiotech | Cat# 1110-05, RRID:AB_2794604 |
| Goat Anti-Mouse IgG, Human ads-HRP | SouthernBiotech | Cat# 1030-05, RRID:AB_2619742 |
| CD326 (EpCAM) Monoclonal Antibody (G8.8), APC | eBioscience | Cat# 17-5791-82 |
| PE anti-mouse CD45 Antibody | Biolegend | Cat# 103106 RRID: AB_312971 |
| FITC anti-mouse I-A/I-E Antibody | Biolegend | Cat# 107606 RRID: AB_313321 |
| FITC anti-mouse TCR β chain Antibody | Biolegend | Cat# 109206 RRID: AB_313429 |
| Alexa Fluor® 647 anti-mouse FOXP3 Antibody | Biolegend | Cat# 126408 RRID: AB_1089115 |
| ROR gamma (t) Monoclonal Antibody (AFKJS-9), PE | eBioscience | Cat# 12-6988-82 |
| Anti-mouse CD4 APC (clone GK1.5) | Biolegend | Cat# 100412, RRID:AB_312697 |
| Anti-mouse CD45.2 APC-Cy7 (clone 104) | Biolegend | Cat# 109824, RRID:AB_830789 |
| Anti-mouse CD4 PerCP-Cy5.5 (clone GK1.5) | Biolegend | Cat# 100434, RRID:AB_893324 |
| Anti-mouse CD4 FITC (clone GK1.5) | Biolegend | Cat# 100406, RRID:AB_312691 |
| Pacific Blue™ anti-mouse CD49b (pan-NK cells) Antibody | Biolegend | Cat# 108918 RRID: AB_2265144 |
| PE/Cyanine7 anti-mouse CD223 (LAG-3) Antibody | Biolegend | Cat# 125226 RRID: AB_2715764 |
| Goat anti-mouse IgG-HRP | Beyotime | Cat# A0216, RRID:AB_2860575 |
| Goat anti-rabbit IgG-HRP | Beyotime | Cat# A0208, RRID:AB_2892644 |
| Ultra-LEAF™ Purified anti-mouse CD3 (clone 172) | Biolegend | Cat# 100253, RRID:AB_2810314 |

(*Continued on next page*)

*Continued*

| REAGENT or RESOURCE | SOURCE | IDENTIFIER |
|---|---|---|
| Ultra-LEAF™ Purified anti-mouse CD28 (clone 37.51) | Biolegend | Cat# 102121, RRID:AB_2810330 |
| **Bacterial and virus strains** | | |
| *Citrobacter rodentium* | ATCC | DBS100 |
| *Listeria monocytogenes* | ATCC | ATCC19115 |
| E. coli BL21(DE3) | New England Biolabs | Cat# C2527 |
| E. coli DH5-alpha | New England Biolabs | Cat# C2987 |
| **Biological samples** | | |
| Fetal Bovine Serum | Thermo Fisher Scientific | Cat# 10091148 |
| **Chemicals, peptides, and recombinant proteins** | | |
| Ac-DEVD-CHO | selleckchem | Cat#: S7901 |
| Albumin from chicken egg white | Sigma-Aldrich | A5503 |
| Gasdermin D (GSDMD) (NM_024736) Human Recombinant Protein | OriGene | Cat#: TP761411 |
| Recombinant human Caspase-1 protein (Active) | Abcam | ab39901 |
| Recombinant Human Cleaved Caspase-3 protein (active) | Abcam | Cat#: ab52101 |
| Recombinant Human Caspase-7 protein | Abcam | Cat#: ab198478 |
| HEPES | Sigma-Aldrich | Cat#: H3375 |
| DTT for biochemistry | BioFroxx | 3483-12-3 |
| 0.5M EDTA PH8.0 | Biosharp | BL581A |
| Collagenase from *Clostridium histolyticum* | Sigma-Aldrich | Cat#: C6885 |
| DNase 1 | Roche | Cat#: 11284932001 |
| Cholera toxin from *Vibrio cholerae* | Sigma-Aldrich | C8052-2MG |
| Gibco™ BASIC DMEM, High Glucose, Pyruvate | Gibco | C11995500BT |
| RPMI 1640 medium | Thermo Fisher Scientific | Cat# 22400089 |
| Red Blood Cell Lysis Buffer | Biosharp | BL503A |
| DAPI | Biolegend | Cat#: 422801 |
| Propidium Iodide | Beyotime | Cat#: ST511 |
| 7-AAD Viability Staining Solution | Biolegend | Cat# 420403 |
| Penicillin-streptomycin | Gibco | Cat# 10378016 |
| Incomplete Freund's adjuvant | Difco Laboratories | Cat# BD 263910 |
| Mycobacterium tuberculosis H37RA | Difco Laboratories | Cat# BD 231141 |
| Pertussis toxin | List Biological | Cat# 180 |
| Immobilon Western Chemiluminescent HRP Substrate | Millipore | WBKLS0500 |
| Annexin V Alexa Fluor® 647 | Biolegend | Cat# 640943 |
| Opti-MEM | Thermo Fisher Scientific | Cat#: 32985070 |
| PBS | Thermo Fisher Scientific | Cat#: 10010023 |
| Lipofectamine 2000 | Thermo Fisher Scientific | Cat#: 11668019 |
| Lipofectamine 3000 | Thermo Fisher Scientific | Cat#: L3000008 |
| Anti-Flag agrose beads | Sigma-Aldrich | Cat#: A2220 |
| Coomassie brilliant blue R-250, 2X Solution | Sangon Biotech | Cat#: A602151 |
| SM buffer | Gbiosciences | Cat#: 786-491 |
| SYBR™ Green II RNA Gel Stain, 10,000X concentrate in DMSO | Thermo Fisher Scientific | Cat#: S7564 |
| Ribavirin | Selleck | Cat#: S2504 |

(*Continued on next page*)

*Continued*

| REAGENT or RESOURCE | SOURCE | IDENTIFIER |
|---|---|---|
| Acyclovir | Selleck | Cat#: S1807 |
| Lamivudine | Selleck | Cat#: S1706 |
| SYBR qPCR Master MIX | Vazyme | Q311-02 |
| HiScript® III RT SuperMix for qPCR | Vazyme | R323-01 |
| TRNzol Universal Reagent | TIANGEN | Cat#: 4992730 |
| Glutathione Beads | Smart-Lifesciences | Cat#: SA008005 |
| Dextrin Beads | Smart-Lifesciences | Cat#: SA077005 |
| BSA | Sigma-Aldrich | Cat#: A1933 |
| Recombinant Mouse GM-CSF (carrier-free) | Biolegend | Cat#: 576306 |
| Recombinant Mouse M-CSF Protein | R&D Systems | Cat #: 416-ML |
| Standard LPS, E. coli 0111: B4 | invivogen | Cat#: tlrl-eblps |
| Nigericin sodium salt; Potassium ionophore | InvivoGen | Cat#: tlrl-nig |
| Recombinant Mouse IFN-γ (Animal-Free) | Biolegend | Cat#: 714006 |
| **Critical commercial assays** | | |
| Mouse IL-18 ELISA kit | Invitrogen | Cat#: BMS618 |
| Mouse IL-1 beta/IL-1F2 DuoSet ELISA | R&D Systems | DY401 |
| Mouse OVA-specific IgE (OVA-sIgE) ELISA Kit | Shanghai Enzyme-linked Biotechnology | ml063583 |
| Mouse OVA-specific IgG1 (OVA-sIgG1) ELISA Kit | Shanghai Enzyme-linked Biotechnology | ml037615 |
| MCPT-1 (mMCP-1) Mouse Uncoated ELISA Kit | Invitrogen | 88-7503-88 |
| Fixation/Permeabilization Solution Kit | BD Bioscience | Cat# 554714 |
| Cell Stimulation Cocktail (plus protein transport inhibitors) | eBioscience | Cat# 00-4975-93 |
| eBioscience™ Foxp3 / Transcription Factor Staining Buffer Set | eBioscience | Cat# 00-5523-00 |
| Nuclear and Cytoplasmic Protein Extraction Kit | Beyotime | Cat# P0028 |
| Zombie Aqua™ Fixable Viability Kit | Biolegend | Cat# 423102 |
| Pierce Silver Stain Kit | Thero Fisher scientific | Cat#:24612 |
| Mouse Interferon γ, IFN-γ ELISA Kit | Cusabio | CSB-E04578m |
| **Deposited data** | | |
| RNA sequencing data | This paper | SRA:PRJNA923771; GSA: PRJCA017570 |
| Single cell RNA sequencing data | This paper | SRA:PRJNA923771; GSA: PRJCA017570 |
| **Experimental models: Cell lines** | | |
| HEK293T cells | ATCC | CRL-3216 |
| Immortalized BMDMs | Rongbin Zhou Lab | N/A |
| Hela cells | ATCC | CCL-2 |
| MC38 cells | Lieping Chen Lab | N/A |
| BO4 cells | Peter Cresswell Lab | N/A |
| **Experimental models: Organisms/strains** | | |
| *Gsdmd*$^{3xflag}$ mice | Richard Flavell Lab | N/A |
| *Gsdmd*$^{ha}$ mice | Richard Flavell Lab | N/A |
| *Gsdmd*$^{SICR}$ mice | This paper | N/A |
| *Asc*$^{-/-}$ mice | Rongbin Zhou Lab | N/A |
| *Gsdmd*$^{-/-}$ mice | Richard Flavell Lab | N/A |
| *Gsdmd*$^{f/f}$ mice | Feng Shao Lab | N/A |
| *Vil-cre* mice | Rongbin Zhou Lab | N/A |
| *Cd11c-cre* mice | Rongbin Zhou Lab | N/A |

(*Continued on next page*)

| Continued | | |
|---|---|---|
| REAGENT or RESOURCE | SOURCE | IDENTIFIER |
| *H2-Ab1*$^{f/f}$ mice | The Jackson Lab | RRID:IMSR_JAX:013181 |
| *Caspase-1*$^{-/-}$ mice | Rongbin Zhou Lab | N/A |
| *Caspase-11*$^{-/-}$ mice | Rongbin Zhou Lab | N/A |
| *Il-10-GFP* mice | Richard Flavell Lab | N/A |
| *Foxp3-IRES-mRFP mice* | Richard Flavell Lab | N/A |
| *Il27ra*$^{f/f\ cd4\text{-}cre}$ mice | Zhinan Yin Lab | N/A |
| C57BL/6JGpt | GemPharmatech | Strain NO. N000013 |
| Oligonucleotides | | |
| qPCR primers for indicated genes | This paper | See STAR Methods Table |
| ChIP-qPCR primers for indicated genes | This paper | See STAR Methods Table |
| Recombinant DNA | | |
| pCMV6- Myc-DDK - Mouse caspase 3 | Origene | MR203736 |
| pCMV6- Myc-DDK - Mouse caspase 7 | Origene | MR204235 |
| pCDNA3.1-Flag-mGSDMD-HA | This paper | N/A |
| pCDNA3.1-Flag-mGSDMD(D88A)-HA | This paper | N/A |
| pCDNA3.1-3XFlag-mGSDMD-$N_{13}$ (1-88) | This paper | N/A |
| pCDNA3.1-mGSDMD-$C_{42}$ (89-487)-HA | This paper | N/A |
| pCDNA3.1-Flag-mGSDMD (1-192)-HA | This paper | N/A |
| pCDNA3.1-Flag-mGSDMD (89-276)-HA | This paper | N/A |
| pCDNA3.1-GFP-mGSDMD-$N_{13}$ (1-88) | This paper | N/A |
| pCDNA3.1-mCherry-mGSDMD-$N_{13}$ (1-88) | This paper | N/A |
| pCDNA3.1-GFP-mGSDMD-$C_{42}$ (89-487) | This paper | N/A |
| pCDNA3.1-mCherry-mGSDMD-$C_{42}$ (89-487) | This paper | N/A |
| pCDNA3.1-mGSDMD-$N_{30}$ (1-276) | This paper | N/A |
| pCDNA3.1-mCASP-1-HA | This paper | N/A |
| pET-21a-GST-mGSDMD | This paper | N/A |
| pET-21a-MBP-mGSDMD | This paper | N/A |
| pET-21a-MBP-mGSDMD-$N_{13}$ (1-88aa) | This paper | N/A |
| pCDNA3.1-Flag-mGSDMD | This paper | N/A |
| pCDNA3.1-Flag-mSTAT1 | This paper | N/A |
| pCDNA3.1-HA-mGSDMD-$N_{13}$ (1-88aa) | This paper | N/A |
| pLVX-mCherry-mGSDMD | This paper | N/A |
| pLVX-mCherry-mGSDMD-$N_{13}$ (1-88aa) | This paper | N/A |
| pCDNA3.1-HA-hNup98 | This paper | N/A |
| pCDNA3.1-HA-hNup107 | This paper | N/A |
| pCDNA3.1-HA-hNup155 | This paper | N/A |
| pCDNA3.1-HA-mRFX5 | This paper | N/A |
| pSPAX2 | Addgene | 12260 |
| pMD2.G | Addgene | 12259 |
| PLKO.1-shNup98/107/155 | This paper | N/A |
| Software and algorithms | | |
| ImageJ | NIH | https://imagej.nih.gov/ij/ |
| ZEN (black edition) v2.3 | USTC | N/A |
| FlowJo software version 10.6.2 | FlowJo,LLC | https://www.flowjo.com/ |
| Prism version 9 | Graphpad | https://www.graphpad.com/ |
| Image-Pro Plus 6.0 | Image-Pro Plus | https://www.mediacy.com/company/about |

(*Continued on next page*)

*Continued*

| REAGENT or RESOURCE | SOURCE | IDENTIFIER |
|---|---|---|
| Image Lab 5.2.1 | Image Lab | https://www.bio-rad.com/en-hk/product/image-lab-software?ID=KRE6P5E8Z |
| SnapGene 3.2.1 | SnapGene | https://www.snapgene.com/ |
| Bio-Rad CFX Manager 3.1 | Bio-Rad CFX Manager | https://www.bio-rad.com/en-hk/sku/1845000-cfx-manager-software?ID=1845000 |
| R v4.1.1. | R core | https://www.rproject.org/ |
| Seurat v4.0.5 | Stuart, T. et al.[53] | https://satijalab.org/seurat/ |
| CellRanger v3.0.2 | Zheng, G.X. et al.[54] | http://support.10xgenomics.com/single-cell-gene-expression/ software/overview/welcome |
| DESeq2 | Love, M.I. et al.[55] | https://bioconductor.org/packages/release/bioc/html/DESeq2.html |
| STAR | Dobin, A. et al.[56] | https://github.com/alexdobin/STAR |
| RStudio | RStudio Team, 2021 | http://www.rstudio.com/ |
| cNLS Mapper | Kosugi, S. et al.[57] | https://nls-mapper.iab.keio.ac.jp/cgi-bin/NLS_Mapper_form.cgi |
| PredictNLS | GNU Free Documentation License 1.2 | https://rostlab.org/owiki/index.php/PredictNLS |
| DeepLoc-1.0 | DTU Health Tech | https://services.healthtech.dtu.dk/service.php?DeepLoc-1.0 |
| PSORT | Genscript | https://www.genscript.com/psort.html |
| NLStradamus | Nguyen Ba, A.N. et al.[58] | http://www.moseslab.csb.utoronto.ca/NLStradamus/ |
| CaseViewer 2.4 | 3DHISTECH | https://www.3dhistech.com/solutions/caseviewer/ |
| Other | | |
| Immobilon®-P PVDF membrane | Millipore | IPVH00010 |
| 0.02-μm Anodisc polycarbonate filter | Whatman | 6809-7003 |

## RESOURCE AVAILABILITY

### Lead contact

Further information and requests for resources and reagents should be directed to and will be fulfilled by the lead contact, Shu Zhu (zhushu@ustc.edu.cn).

### Materials availability

This study did not generate new unique reagents.

### Data and code availability

The raw data of bulk RNA-seq and scRNA-seq have been deposited in the NCBI BioProject repository and processed data have been deposited in the Genome Sequence Archive at BIG Data Center, Beijing Institute of Genomics (BIG), Chinese Academy of Sciences. These data are publicly available as of the date of publication. Accession numbers are listed in the key resources table. Original western blot images and microscopy data reported in this paper will be shared by the lead contact upon request. This paper does not report an original code. Any additional information required to reanalyze the data reported in this work paper is available from the Lead Contact upon request.

## EXPERIMENTAL MODEL AND STUDY PARTICIPANT DETAILS

### Mice

All mice were maintained in a strict 12 h light cycle under SPF condition. All mouse strains used in this paper are on C57BL/6 background. The co-housing littermate mice were used as the controls in most of the studies unless otherwise indicated. All experiments

were done in an age and sex matched manner. 6-8 weeks old male or female mice were used in most of the studies except for those with peanut allergy models (5-week-old) or those fed with AA food (weaning). Two sgRNAs and one ssDNA contains mutation of GSDMD amino acids DVVD (85-88) to AAAA were used to generate $Gsdmd^{SICR}$ mutant strain by CRISPR–Cas9 technology. 5' 3XFlag-*Gsdmd*, 3' HA-*Gsdmd*, $Gsdmd^{-/-}$, and *H2-Ab1* floxed mice were provided by Dr. Richard Flavell, *Cd11c*-cre, *Villin*-cre mice were provided by Dr. Rongbin Zhou. Gsdmd floxed mice were provided by Dr. Feng Shao. *Il27ra floxed CD4*-cre mice were provided by Dr. Zhinan Yin. All animal experiments were approved by the Ethics Committee of University of Science and Technology of China (USTCACUC172101054).

### Cell culture

Murine colon adenocarcinoma cells MC38 cells, murine bone marrow cells immortalized BMDM (iBMDM) cells and human embryonic kidney 293T (HEK293T) cells, human female cervical cancer cells Hela cells were cultured in DMEM with 10% FBS, 1% penicillin-streptomycin, incubated in 5% CO2 incubator at 37 °C. BO4 cells were cultured in RPMI-1640 with 10% FBS, 2 mM L-glutamine, 1% penicillin-streptomycin, 50 μM 2- mercaptoethanol and 1 mM pyruvate incubated in 5% CO2 incubator at 37 °C. These cell lines are not listed in the database of commonly misidentified cell lines maintained by the ICLAC (International Cell Line Authentication Committee), and not authenticated or tested for mycoplasma contamination.

## METHOD DETAILS

### Immunoprecipitation and western blot analysis

HEK293T cells transfected with indicated plasmids or upper small intestine IECs were harvested and resuspended in 1 ml ice-cold Pierce IP buffer containing protease inhibitors (Complete Mini EDTA-free PMSF, and phosphatase inhibitor (NaF and $NaVO_3$)). Cells were lysed on ice for 20 min then centrifuge at 15,000 g for 10 min to harvest the supernatant. Set aside 10 percent of lysate as input. For each IP sample, add 20-40 μL anti-Flag M2 beads to the rest of cell lysate and incubated overnight. Beads were washed five times with immunoprecipitation buffer and, finally, the bound proteins eluted by boiling in loading buffer.

Samples were separated on 8%-15% Tris-Bis gels and transferred onto PVDF membranes. Western blot analysis was performed using antibodies against Flag, HA, GSDMD, ACTIN, MYC, CASPASE-1/3/7 (key resources table).

### Isolation of IECs and IELs in the intestine

Small intestines were excised and flushed thoroughly three times with PBS. They were turned inside out and cut into ~1 cm sections then transferred into RPMI with 2 mM EDTA, and shaken for 20 min at 37 °C. Supernatants were collected through a 100-mm cell strainer to get single-cell suspensions. Cells were collected as the IEC fraction which contains both epithelial cells (~90%) and lymphocytes (IEL, ~10%). Single-cell suspension was used for further analysis.

### Isolation of lamina propria lymphocytes in the intestine

Small intestines were excised and flushed with PBS to flush off the intestinal content. They were turned inside out and cut into ~1 cm sections after removing payer's paches. These sections then were transferred into RPMI with 2 mM EDTA, and shaken for 15 min at 37 °C for 3 times. And the supernatants were discarded. Collect tissue sections and washed with RPMI (EDTA free) for another 5 min. The intestinal sections were transferred into digestion buffer (RPMI with 0.5 mg/ml collagenases II, 0.5 mg/ml Dnase I and 5% FBS) (key resources table) and shaken for 20 min at 37 °C. Stop the digestion by adding EDTA to the digestion buffer. Supernatants were collected through a 100-mm cell strainer to get single-cell suspensions as lamina propria lymphocytes (LPL).

### ABX Treatment

C57BL/6 wild-type mice were supplied with a mixture of antibiotics (ampicillin 1mg/mL, neomycin 1mg/mL, metronidazole 1mg/mL, and vancomycin 0.5 mg/mL) (key resources table) in drinking water for 4 weeks. Fresh feces samples were collected for the measurement of fecal bacteria load.

### AVC Treatment

Wild-type mice were orally supplied with ribavirin (30 mg/kg), lamivudine (10 mg/kg) and aciclovir (20 mg/kg) (key resources table) via i.g once a day for 3 weeks. Fecal virus-like particles were determined subsequently. 0.1g feces was suspended in 2ml sterilized SM buffer. Subsequently, feces samples were centrifuged at 2500g ,4°C for 10min, and filtered through 0.45μm (Millex-HV) and 0.22μm filters (Millipore) to remove cell debris and bacteria. Filtrates were filtered on to a 0.02-μm Anodisc polycarbonate filter. Filters with viral particles were stained with 10× SYBR Green II for 15 min. After that, the filters were washed once and imaged at a ×40 magnification. Stained particles <0.5 μm in diameter were regarded as VLPs.

### Bile duct ligation

The common bile ducts in pentobarbital-anesthetized wild-type mice were exposed in after midline laparotomy, followed by double ligation with 6-0 silk sutures. The abdomen was properly closed and the mice were put on a heat pad for recovery. Two weeks later, the mice were sacrificed and tissues were harvested for further analyses.

### AA food

AA food was customized by Medicience (Jiangsu, CN). The AA food ingredient was listed as follows (g/kg): L-Alanine 4.5; L-Arginine, 6.3; L-Aspartic Acid 11.3; L-Cystine 3.7; L-Glutamic Acid 36.2; Glycine 3.1; L-Histidine, 4.5; L-Isoleucine 8.4; L-Leucine 15.3; L-Lysine-HCl 16.1; L-Methionine 4.5; L-Phenylalanine 8.7; L-Proline 20.4; L-Serine 9.4; L-Threonine 6.6; L-Tryptophan 2.1; L-Tyrosine 9.2; L-Valine 9.9; Sucrose 100; Cornstarch 399.886; Dyetrose 145; Soybean Oil 70; tBHQ 0.014; Cellulose 50; Salt Mix 35; Sodium Bicarbonate 7.4; Vitamin Mix 10; Choline Bitartrate 2.5. All diets were irradiated and vacuum-packed. The feeding method of AA food to mouse starts at 3-4 weeks of age and continued for 3-6 weeks. All mice were allowed free access to water.

### Bacterium infection

For *C. rodentium* and *L. monocytogenes* infection, 6-week-old wild type mice were intragastrically (i.g.) infected with $1 \times 10^{11}$ or $1 \times 10^{10}$ CFU·kg$^{-1}$ bacteria (key resources table). On the 7th day, the mice were sacrificed, and the duodenum IECs were removed for western blotting.

### IP-MS

GST-GSDMD and MBP-GSDMD 1-88aa were expressed in BL21 (key resources table), and purified with Glutathione Beads or Dextrin Beads; biotinylated OVA peptides (synthesized by Top-Peptide BioCoLtd) were conjugated to Streptavidin beads followed by double ligation with 6-0 silk sutures. These purified proteins/peptides ligated on beads were then incubated with IEC cell lysates for 2 hours. 3XFlag-GSDMD were expressed in HEK293T cells and cell lysates were incubated with anti-Flag beads. Beads were then washed and finally boiled in loading buffer.

Samples were separated in 8% or 15% Tris-Glycine gels and stained with Coomassie brilliant blue. Specific bands were cut and digested with trypsin to perform Mass spectrometry (aptbiotech, Shanghai CN).

### *Ex vivo* GSDMD cleavage by CASP-7

Isolated duodenum IEC lysates from NCD- or AAD- fed mice were mixed with lysates of HEK293T cells transduced with Myc-Flag-*Casp7* and Flag-*Gsdmd*-HA plasmids, and incubate for 15 minutes at 37 °C. Cleavage of CASP-7 and GSDMD were first pulled down by Flag-beads and then examined by western blots.

### *In vitro* GSDMD cleavage by recombinant caspases

As described by Jianjin Shi et al.,[14] purified recombinant human GSDMD (key resources table) was incubated with human CASP-1, 3 and 7 (key resources table) in a 25μl reaction containing 50 mM HEPES (pH 7.5), 3 mM EDTA, 150 mM NaCl, 0.005% (vol/vol) Tween-20 and 10 mM DTT. The reaction was incubated for 60 min at 37 °C. Cleavage of GSDMD was examined by Silver-staining of the reaction samples separated on the 15% SDS–PAGE gel.

### OVA peptides binding assay

Upper small intestine IECs from wild-type mice or HEK293T cells transfected with *Caspase-7* plasmids were harvested and resuspended in 1 ml IP buffer containing protease inhibitors and incubated on ice for 20 min. Then centrifuge at 15,000 g for 10 min and collected supernatant. Then supernatants were incubated with indicated biotinylated OVA peptides with different length and sequence (synthesized by Top-Peptide BioCoLtd) and Streptavidin beads for 6 hours at 4°C, beads were then washed and finally boiled in loading buffer.

### *In vitro* caspases cleavage assay by OVA peptides

The Biotin-OVA (323-330) peptide, biotin-OVA (323-339) peptide or biotin-ctrl peptide were ligated with streptavidin beads first, and then incubated with purified recombinant CASP-3/7 for 4 hours at 4°C. Beads were then washed and boiled in loading buffer. Samples were immunoblotted with anti-CASP-3 or CASP-7 antibody.

### Chromatin Immunoprecipitation (ChIP)-qPCR

The DNA preparation from upper small intestine IECs from indicated mice in Figure 3S and T or HEK293T cells transfected with indicated plasmids in Figure 3Q and R, the cross-linking, and immunoprecipitation with indicated antibodies followed the manufacturer's protocols of NovoNGS® CUT&Tag 3.0 High-Sensitivity Kit (Novoprotein N259-YH01) or ChIP Assay Kit (Beyotime P2078). The samples were then subjected to qPCR with indicated primers. Data were normalized to the value of the group HEK293T cells transfected with empty-vector plasmids, or the value of the group immunoprecipitated with control IgG.

| ChIP-qPCR primers | IDENTIFIER |
|---|---|
| *hCIITA*-ChIP-Forward1: CTGTGAGGAACCGACTGGAG | N/A |
| *hCIITA*-ChIP-Reverse1: GGAGCAACCAAGCACCTACT | N/A |
| *mCiita*-ChIP-Forward: GGCTCAAATCTGTCGTCCTCT | N/A |
| *mCiita*-ChIP-Reverse: TTCCAGAGGACCCCTCCCTA | N/A |
| *hCIITA*-ChIP-Forward2: CCCAACAGACTTTCTGTGCAAC | N/A |
| *hCIITA*-ChIP-Reverse2: ACCACACTCCCTTAAGCCCT | N/A |
| *hGAPDH*-ChIP-Forward: TACTAGCGGTTTTACGGGCG | N/A |
| *hGAPDH*-ChIP-Reverse: TCGAACAGGAGGAGCAGAGAGCGA | N/A |
| *mGapdh*-ChIP-Forward: AGAGAGGGAGGAGGGGAAATG | N/A |
| *mGapdh*-ChIP-Reverse: AACAGGGAGGAGCAGAGAGCAC | N/A |

### Preparation of purified peanut allergens

The peanut extracts was prepared as described before.[59] Briefly, peanuts were ground and the protein was extracted by mixing 25g ground peanut with 20ml 20mM Tris-HCl buffer (pH 7.2). After this mixture was stirred for 2h at room temperature, the aqueous fraction was collected by centrifugation (3000g for 30 min) and subsequently centrifuged at 10,000 g for 30 min to remove residual traces of fat and insoluble particles. The extracts contain 30 mg/ml protein was determined by BCA analysis.

### Peanut allergy mouse model

The orally administrated peanut allergy model was performed as described before.[60] Briefly, 5 weeks old male or female mice were sensitized 5 times, 1 weeks apart, with 6 mg of peanut (PN) in the presence of 10 μg cholera toxin (CT, Sigma-Aldrich) via intragastric gavage. Five weeks later, mice are orally administered 20 mg of PN twice 30 min apart. Rectal temperature was recorded every 5 minutes for 1 hour right after the 2$^{nd}$ challenge, the serum was collected after temperature recording for the measurements of mMCP-1. The mouse was sacrificed the next day and serum was collected for the measurements of PN-sIgE and PN-sIgG, the duodenum IECs was coolected for the measurements of MHCII molecules by FACS. Before each intragastric gavage challenge, mice are deprived of food for 4 hours and gavaged with 200μl 0.2M sodium bicarbonate ($NaHCO_3$, dissolved in sterilized dd$H_2O$) 30 minutes before allergens gavage.

mMCP-1 was detected using the MCPT-1 mouse uncoated ELISA kit (key resources table) following the manufacturer's protocol. For PN-specific ELISAs, plates were coated overnight at 4°C with 50μg/mL Peanut extracts in 100mM carbonate-bicarbonate buffer (pH 9.6). Plates were blocked for 2 hours at room temperature with 3% BSA. Samples were added in 1% BSA (1:10 diluent for IgE and 1:500 diluent for IgG) and incubated overnight at 4°C. Peanut-specific IgE/G were detected using goat anti-mouse IgE-HRP or goat anti-mouse IgG-HRP (key resources table) and TMB liquid substrate system (key resources table) for ELISA. The plates were read in an ELISA plate reader at 450 nm.

### Delayed type hypersensitivity (DTH) mouse model

6-7 weeks old male or female mice were fed with 20 mg of OVA in 200 μl DPBS via intragastric gavage on days 1, 4, and 7. On day 14, mice were immunized subcutaneous injection with 50 ug OVA in 100 ul PBS-CFA emulsion. Mice were challenged subcutaneously with 250 ug heat-aggregated OVA in 20 ul of PBS in the left hind footpad and 20 ul PBS in the right footpad as a control 7 days later. OVA-specific DTH was determined by footpad swelling 24 hr after challenge. Footpad swelling was measured as difference in the thickness of OVA-challenged and PBS-injected control footpad for each mouse.

Total splenocytes were subsequently isolated, seeded in a 96-well plate, and stimulated *in vitro* with 1 mg/ml OVA. 4 days later, supernatants were collected for the measurement of IFNγ by ELISA (key resources table).

### Flow cytometry and cell sorting

Single-cell suspensions of IECs, IELs, or LPL were stained with FACS antibodies (key resources table) in FACS buffer (PBS with 2% BSA and 5 mM EDTA) for 20 min at 4°C for surface staining. For intracellular staining, cells were fixed and stained according to the instructions of the Invitrogen (Ebioscience) Fix/Perm Kit.

For FACS sorting, cells were prepared and stained as described and sorted on a BD FACSAria flow cytometer. $CD45.2^{+}$ $EpCAM^{-}$ cells were sorted as IELs, and $CD45.2^{-}$ $EpCAM^{+}$ cells were sorted as IECs.

### Quantitative PCR with reverse transcription

Total RNA was extracted from IECs, LPLs or FACS sorted cells, using trizol reagent. RNA was purified according to the manufacturer's instructions. Reverse transcription procedure was performed according to the instruction of RT kit (key resources table). After RT, qPCR was performed using the CFX384 Real-Time System (Bio-Rad).

Data were analyzed using the Sequence Detection Software according to the ΔCt method. All results were normalized to *Hprt* or *Gapdh* quantified in parallel amplification reactions.

| RT-qPCR primers | IDENTIFIER |
|---|---|
| *mH2-Ab1*-Forward: CACTCTGGTCTGTTCGGTGAC | N/A |
| *mH2-Ab1*-Reverse: CCTCTCCCTGATGAGGGGTC | N/A |
| *mH2-Eb1*-Forward: GCGGAGAGTTGAGCCTACG | N/A |
| *mH2-Eb1*-Reverse: AGGCCCGTGGACACAATTC | N/A |
| *mH2-DMb1*-Forward: ACCCCACAGGACTTCACATAC | N/A |
| *mH2-DMb1*-Reverse: GGATACAGCACCCCAAATTCA | N/A |
| *mH2-Aa*-Forward: CAACCGTGACTATTCCTTCC | N/A |
| *mH2-Aa*-Reverse: CCACAGTCTCTGTCAGCTC | N/A |
| *mCd74*-Forward: TGGAAGATCTTCGAGAGCTGGATG | N/A |
| *mCd74*-Reverse: TTCCTGGCACTTGGTCAGTA | N/A |
| *mHprt*-Forward: CTGGTGAAAAGGACCTCTCGAAG | N/A |
| *mHprt*-Reverse: CCAGTTTCACTAATGACACAAACG | N/A |
| *mGapdh*-Forward: CATCACTGCCACCCAGAAGACTG | N/A |
| *mGapdh*-Reverse: ATGCCAGTGAGCTTCCCGTTCAG | N/A |
| *mIl10*-Forward: GCTCTTACTGACTGGCATGAG | N/A |
| *mIl10*-Reverse: CGCAGCTCTAGGAGCATGTG | N/A |
| *mCiita*-Forward: CCCTGCGTGTGATGGATGTC | N/A |
| *mCiita*-Reverse: ATCTCAGACTGATCCTGGCAT | N/A |

### Immunofluorescent and confocal microscopy

HeLa or HEK293T cells transduced with indicated plasmids were grown on cover slips in 24-well plates. After the corresponding experimental treatment, cells were fixed in 4% paraformaldehyde for 30 min at room temperature then washed with PBS twice. Cells

were mounted with VECTASHIELD Mounting Medium to visualize the nuclei. Images were obtained using a fluorescence microscope (DP72; Olympus).

Mouse intestinal samples were fixed with 4% paraformaldehyde (PFA) and embedded in paraffin. Immunofluorescent staining was done in Servicebio (Wuhan, CN) with primary antibodies (key resources table) we provided. For quantification, 5 randomly selected fields of one biological sample were averaged to obtain a single value and 3 biological replicates were used to compare the differences.

### BMDC culture

Muscles and tissues were debrided from leg bones of 6 weeks old male mice, which were then disinfected in 70% EtOH for 30 sec and washed 3 times with sterilized PBS. The bone marrows were flushed out with a new 1 mL syringe filled with sterilized PBS. Cells were detached by pipetting up and down and the single cell suspension was centrifuged at 1,500 rpm for 5 min, then erythrocytes were eliminated using Red Blood Cell Lysing Buffer and remaining cells were resuspended in RPMI medium supplemented with 10% FBS and 20 ng/mL GM-CSF (key resources table) at a density of 2 x $10^5$ viable cells per mL with a total volume of 10ml in 10 cm plate. Plates were placed in a 37 °C incubator with 5% $CO_2$. Refresh the RPMI medium with 10% FBS and 20 ng/mL GM-CSF on day 3. On day 6, 10 mL cell culture was collected and centrifuged at 1,500 rpm for 5 min. The supernatant was discarded and the cells were resuspended in 10mL RPMI medium supplemented with 10% FBS and 20 ng/mL GM-CSF, and added back to the original plate. Non-adherent and loosely adherent cells in the culture supernatant can be harvested by gentle flushing with PBS on day 8.

For *in vitro* stimulation, 5 × $10^5$ BMDC was plated overnight in 12-well plates and the stimulated with LPS (100ng/ml) or IFN-γ (50ng/ml) (key resources table). Then the cells were harvested at indicated time points for FACS analyses.

### BMDM culture

Muscles and tissues were debrided from leg bones of 6-week-old male littermate $Gsdmd^{WT}$ and $Gsdmd^{SICR}$ mice and control $Gsdmd^{KO}$ mice. Then bone marrow cells from all bones were flushed out. After centrifuging for 5 min at 1500 rpm, Erythrocytes were eliminated using Red Blood Cell Lysing Buffer. The remaining cells were seeded in non-treated 10 cm dishes and incubated in complete DMEM medium with 50 mg/ml recombinant mouse M-CSF for 4 days (change the medium every 2 days) to form proliferative nonactivated cells.

For pyroptosis induction in Figure S2I, BMDMs were primed by LPS (100 ng/ml) for 4 hours and then treated with nigericin (10 μM) (key resources table) for 40 minutes. Supernatant proteins were collected for western blotting to detect GSDMD pyroptotic cleavage and CASP-1 activation. Gray values were measured by Imagej and gray values of pyroptotic forms of GSDMD and CASP-1 were normalized to their precursors for LPS+nig treated BMDMs.

### Antigen presentation assay

To determine whether GSDMD deficiency reduces MHC class II on the cell membrane of IECs or BMDCs, we assayed the presentation of MHC class II-antigen complex by measuring the production of IL-2 by the T cell hybridoma BO4, which specifically recognizes $HEL_{74-88}$ peptide presented by mouse H2-$A^b$. We isolated the IECs or BMDCs from $Gsdmd^{+/+}$, $Gsdmd^{-/-}$ and $H2\text{-}Ab^{\Delta IEC}$ mice. 1*$10^6$ cells were incubated in IEC/DC medium (DMEM with 10%FBS, penicillin-streptomycin) with 10 μg/mL HEL peptide or HEL non-covalently conjugated 3uM beads at 37 °C, 5% $CO_2$ for 3 h. Then IECs or BMDCs were fixed by 0.5% PFA in PBS at 37 °C for 10 min. The fixed cells were washed with 200 mM glycine in PBS twice and followed with IEC/DC medium twice. Then 1*$10^5$ BO4 cells in 200 μL BO4 medium (RPMI-1640 medium supplemented with 10% FBS, 2 mM L-glutamine, penicillin-streptomycin, 50 μM 2- mercaptoethanol and 1 mM pyruvate) were added and incubated together with the IECs or BMDCs at 37 °C, 5% $CO_2$ for 12-14 hours. Then the IL-2 levels in the supernatant were measured by ELISA (key resources table).

### RNA-Seq and data analysis

RNA-Seq library preparation and sequencing for IEC samples from 6 weeks old male $Gsdmd^{+/+}$ or $Gsdmd^{-/-}$ mice were performed by Berrygenomics company (Beijing, CN) on an Illumina 2500 machine. RNA-Seq fastq files were first processed by fastp to remove adaptor and low-quality reads, then aligned to the mm10 mouse genome assembly by STAR (v2.5.3a), followed by quantification with HT-seq (v0.9.0). The resultant gene count data were analyzed with R package. Differentially expressed genes between the experimental groups were identified by edgeR (v3.29.2), and further filtered for at least 1.5-fold changes. Pathway analysis was performed using Metascape. For analysis of antigen presentation signatures, gene set enrichment analysis (GSEA) was performed by using the Broad Institute's GSEA program, using custom gene sets. The set of signature genes were used to generate the heat map.

### Single-cell RNA sequencing

Upper small intestinal tissues were collected and washed in cold PBS several times to remove contents. IEC fraction and LPL were harvested as described above. Mixing LPL and IEC at 1:1 as a cell suspension sample for further single cell library construction. Single-cell RNA-seq libraries and sequencing for samples were performed by Berrygenomics company (Beijing, CN) using the Chromium Single Cell 3' Reagent Kits v3 (10x Genomics), according to the manufacturer's instructions. Briefly, approximately 10$^6$ cells were washed with 0.04% BSA DPBS for three times and were resuscitated to a concentration of 700∼1200 cells/ul (viability ≥ 85%). Cells were captured in droplets at a targeted cell recovery of cells. After the reverse transcription step, emulsions were broken and

Barcoded-cDNA was purified with Dynabeads, followed by PCR amplification. Amplified cDNA was then used for 3'gene expression library construction. For gene expression library construction, 50 ng of amplified cDNA was fragmented and end-repaired, double-size selected with SPRIselect beads, and sequenced on an NovaSeq platform (Illumia) to generate 150 bp paired-end Reads.

Raw reads were demultiplexed and mapped to the reference genome by 10X Genomics Cell Ranger pipeline v3 using default parameters. All downstream single-cell analyses were performed using Cell Ranger and Seurat[61,62] unless mentioned specifically. In brief, for each gene and each cell Barcode (filtered by CellRanger), unique molecule identifiers were counted to construct digital expression matrices. Secondary filtration by Seurat: A gene with expression in more than 3 cells was considered as expressed, and each cell was required to have at least 200 expressed genes. And filter out some of the foreign cells.

Cellranger count takes FASTQ files performs alignment, filtering, Barcode counting, and UMI counting. It uses the Chromium cellular Barcodes to generate feature Barcode matrices by cellranger count or cellranger aggr and reruns the dimensionality reduction, clustering, and gene expression algorithms using cellranger default parameter settings.

Secondary Analysis of Gene Expression we use Seurat. The Seurat package was used to normalise data, dimensionality reduction, clustering,differential expression. we used Seurat alignment method canonical correlation analysis (CCA)[63] for integrated analysis of datasets. For clustering, highly variable genes were selected and the principal components based on those genes used to build a graph, which was segmented with a resolution of 0.6.

## QUANTIFICATION AND STATISTICAL ANALYSIS

The sample size chosen for our animal experiments in this study was estimated based on our prior experience of performing similar sets of experiments. All animal results were included and no method of randomization was applied. For all the bar graphs, data were expressed as mean ± s.e.m. Statistical analyses were performed with a standard two-tailed unpaired Student's *t*-test or paired Student's *t*-test using GraphPad Prism 9. For comparisons between body temperature curves, two-way ANOVA tests were used. To compare two non-parametric data sets, a Mann–Whitney *U*-test was used. $P$ values $< 0.05$ were considered significant. The sample sizes (biological replicates), specific statistical tests used, and the main effects of our statistical analyses for each experiment were detailed in each figure legend.

CellPress

# Supplemental figures

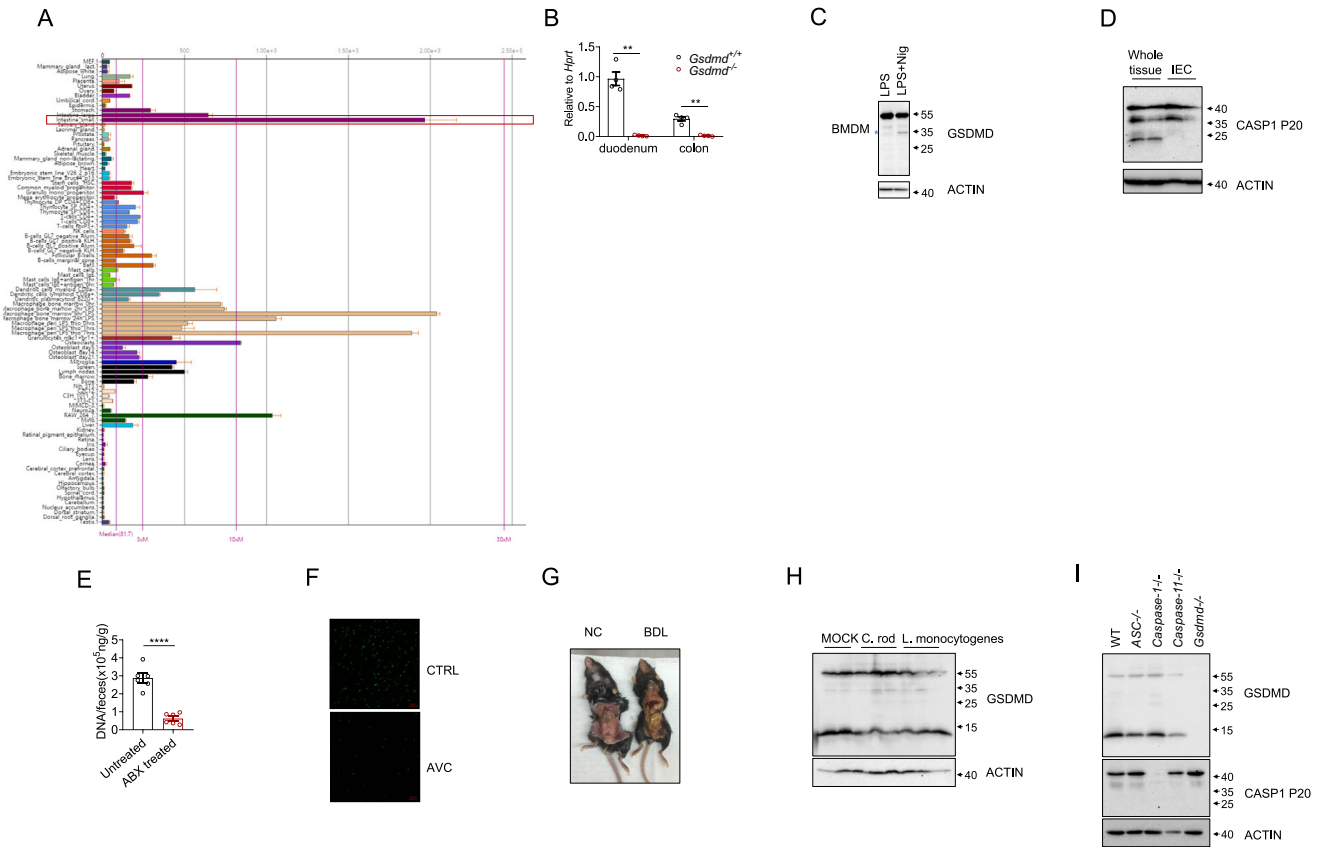


**Figure S1. Dietary antigens induce a non-pyroptotic 13-kD GSDMD fragment in the upper small intestine, related to Figure 1**

(A) *Gsdmd* mRNA expression in different mouse tissues from BioGPS.

(B) qPCR analysis of the *Gsdmd* expression in IECs from indicated intestine sections, the *Gsdmd* expression in *Gsdmd*$^{-/-}$ mice was used as control.

(C) Immunoblotting of GSDMD in BMDM cells lysates treated with pyroptotic stimuli.

(D) CASP-1 cleavage in intestine tissue or IECs. Immunoblotting of CASP-1 in whole intestine tissue or IEC.

(E) Efficacy of the ABX. qPCR measurement of bacterial 16s DNA concentrations in fecal samples from antibiotics (ABX)-treated mice or controls.

(F) Efficacy of the AVC. SYBR green staining of viral particles in fecal samples from antiviral cocktail (AVC)-treated mice or controls.

(G) Efficacy of the BDL treatments. Image of enterocoelia showing acute obstructive jaundice from mice received bile duct ligation (BDL) surgery or control surgery.

(H) Immunoblotting of GSDMD in small intestine from mice infected with enteric bacteria *Citrobacter rodentium* (*C. rod*) or *Listeria monocytogenes* (*L. monocytogenes*).

(I) Immunoblotting of GSDMD in isolated IECs of small intestine from indicated mouse strains with deficiency in inflammasome component.

Data in (B) and (E) are mean ± SEM, for comparisons between two groups, Student's t tests were used **p < 0.01, ****p < 0.0001, (B)–(I) are representative of three independent experiments.

A

| IP-MS Experiment | Candidate Protein | Unique Peptide Count | Coverage (%) | Rank |
|---|---|---|---|---|
| GST-GSDMD+IEC lysate-33kDa | CASP-3 | 4 | 15.16 | 47/2944 |
| GST-GSDMD+IEC lysate-40kDa | CASP-1 | 4 | 10.45 | 90/3901 |
| 293t Flag-GSDMD-40kDa | CASP-7 | 5 | 21.8 | 39/679 |
| 293t Flag-GSDMD-40kDa | CASP-1 | 5 | 12.5 | 59/679 |
| OVA (323-339) +IEC lysate-38kDa | CASP-7 | 12 | 28.38 | 1/3109 |
| OVA (323-339) +IEC lysate-32kDa | CASP-3 | 3 | 11.55 | 35/3917 |
| GSDMD-$N_{13}$+IEC lysate-100kDa | STAT1 | 8 | 10.81 | 137/5096 |
| GSDMD-$N_{13}$+IEC lysate-94kDa | NUP98 | 5 | 3.63 | 156/4882 |
| GSDMD-$N_{13}$+IEC lysate-110kDa | NUP107 | 4 | 4.64 | 113/3123 |
| GSDMD-$N_{13}$+IEC lysate-160kDa | NUP155 | 7 | 6.09 | 52/2954 |
| GSDMD-$N_{13}$+IEC lysate-110kDa | RFX5 | 1 | 1.22 | 1490/3123 |

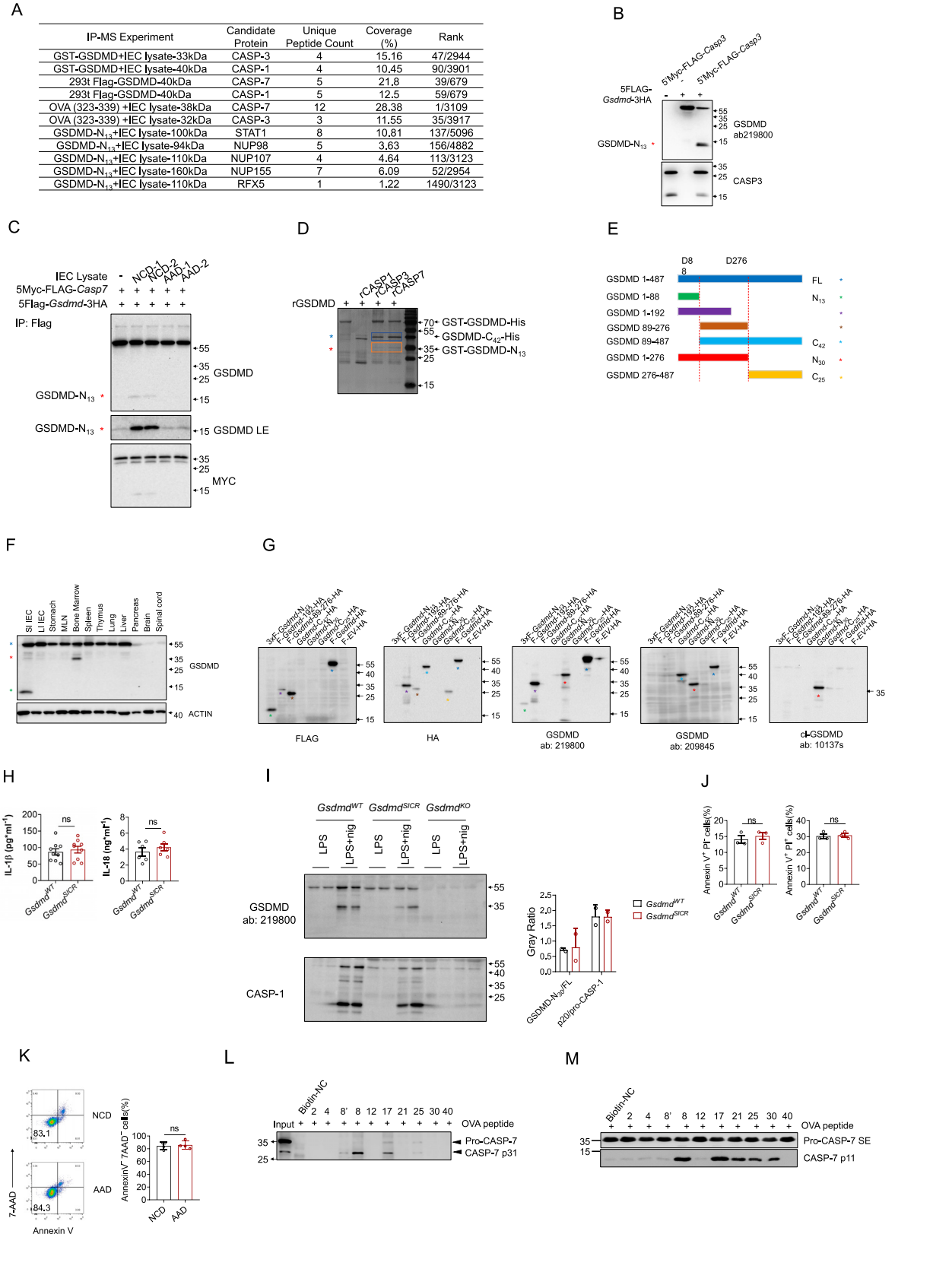


(legend on next page)

**Figure S2. Caspase-7 and caspase-3 cleave GSDMD at D88 in duodenum IECs in response to dietary antigens, related to Figure 2**

(A) List of candidates' unique peptide counts, coverages and ranks that are identified by aforementioned IP-MS analysis in Figures 2A, 2B, 2N, 3O, S3H, and S3P.

(B) GSDMD cleavage induced by CASP-3 in HEK293T cells.

(C) The effects of AAD diet on the cleavage of GSDMD and CASP-7, by co-culturing of IEC lysates with HEK293T cell lysates transfected with indicated plasmids.

(D) *In vitro* incubation of purified recombinant GSDMD with indicated recombinant caspases.

(E) Diagram of the GSDMD truncations.

(F) Labeling of GSDMD truncations in Figure 1A.

(G) Validation of the targeted region of GSDMD antibodies or tag antibodies.

(H) Inflammatory factors IL-1β and IL-18 produced by duodenum explants from indicated mice.

(I) Pyroptosis induction in BMDM. Gray values were measured by ImageJ and the pryroptotic forms of GSDMD and CASP-1 were normalized to their precursors.

(J and K) Death staining in IECs. FACS staining of annexin V and PI for duodenum epithelial cells from *Gsdmd*$^{SICR}$ mutant mice or the littermate WT control mice (J), or from NCD or AAD-fed mice (K).

(L and M) Mapping of biotin-OVA peptides that bind to CASP-7 in HEK293T cells (L) or induce CASP-7 activation in HEK293T cells (M). The sequences of OVA peptides were listed in Figure 2Q.

Data in (H–K) are mean ± SEM, for comparisons between two groups, Student's t tests were used; ns, not significant, (B–M) are representative of three independent experiments.

See also Table S1.

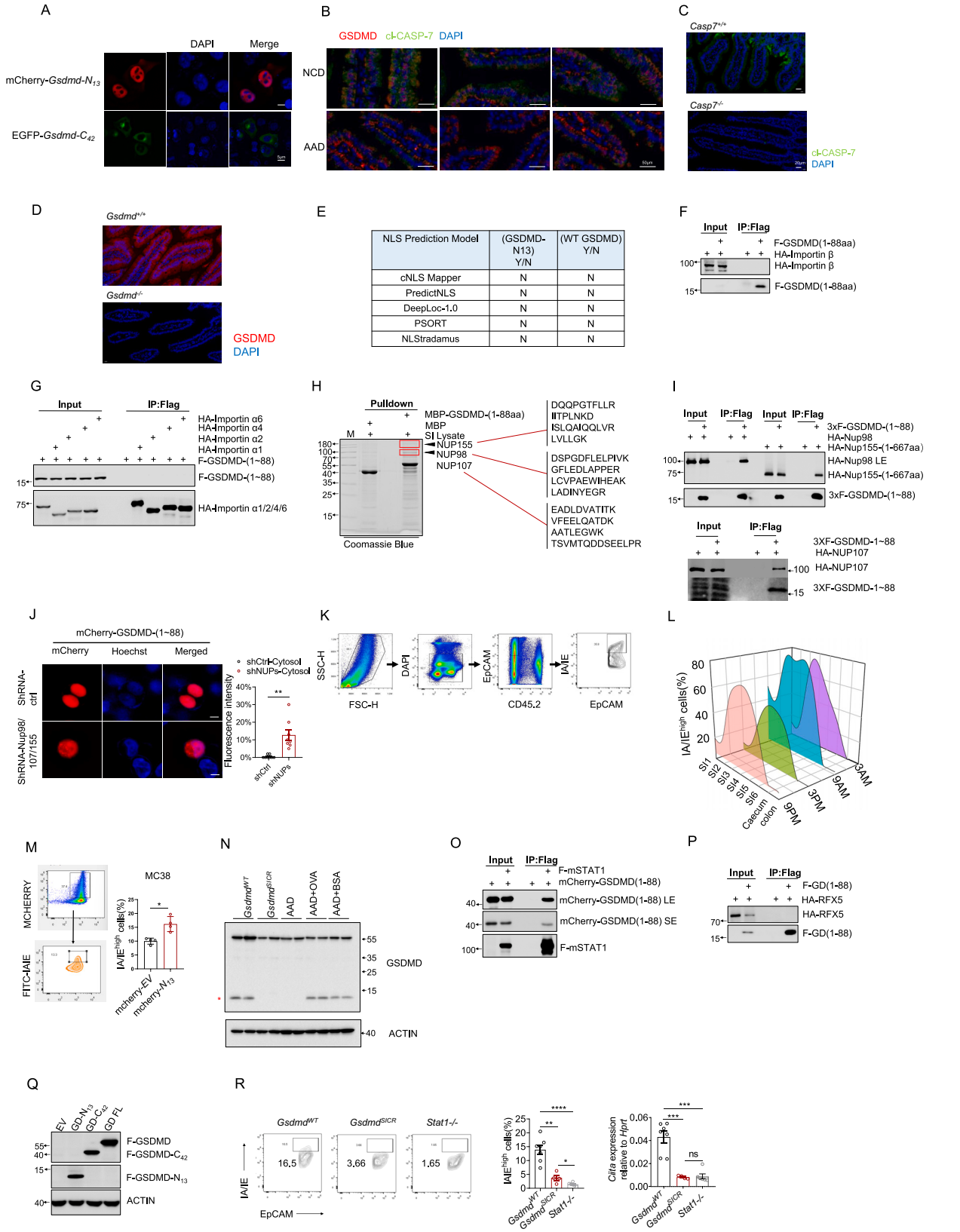


(legend on next page)

**Figure S3. The nuclear-localized GSDMD fragment assists STAT1 to induce CIITA and MHCII in IECs, related to Figure 3**

(A) Confocal images of HEK293T cells transfected with indicated florescence-fused GSDMD fragments.

(B) Immuno-fluorescence of GSDMD and cleaved-CASP-7 in duodenum from 3 pairs of NCD or AAD-fed mice, related to Figure 3C.

(C and D) Verification of the specificities of primary antibodies for XXXmmune-fluorescence (IF) assay used in Figures 3C and S3B.

(E) NLS prediction for GSDMD by multiple tools.

(F and G) CoIP of GSDMD-$N_{13}$ with Importin β (F), or with Importin α (G) in HEK293T cells.

(H) MBP-GSDMD-$N_{13}$ pull-down assay with IEC lysates, the same experiment shown in Figure 3O.

(I) CoIP of GSDMD-$N_{13}$ and NUP98/NUP107/NUP155 in HEK293T cells.

(J) Confocal images of florescence-fused GSDMD-$N_{13}$ in HEK293T cells transduced with shRNAs targeting NUP98/NUP107/NUP155 or control shRNA. Each dot represents a single cell in the quantification.

(K) Gating strategy of MHCII staining in IECs.

(L) MHCII staining of IECs from different intestine segments at different time points of a day, small intestines were divided to 6 equal-length segments and named as SI1 (next to stomach) -SI6 (next to caecum).

(M) FACS staining of MHCII in MC38 cells transfected with GSDMD-$N_{13}$ or control plasmids.

(N) Western blot for GSDMD cleavage in duodenum from AAD-fed mice re-administrated with 20 mg/mL OVA or BSA for 1 week (related to Figure 3H).

(O and P) CoIP of GSDMD-$N_{13}$ and STAT1 (O), or with RFX5 (P) in HEK293T cells.

(Q) Western blot was performed to evaluation the expression levels of the GSDMD truncations in Figure 3Q.

(R) FACS staining of MHCII molecules and qPCR analysis of *Ciita* in duodenum IECs from *Gsdmd*$^{SICR}$ mutant mice, *Stat1*$^{-/-}$ mice or their WT control mice.

Data in (J), (M), and (R) are presented as the mean ± SEM, for comparisons between two groups, Student's t tests were used; for more than two groups, analysis of variance (ANOVA) was used; ns, not significant, *$p < 0.05$, **$p < 0.01$, ***$p < 0.001$, and ****$p < 0.0001$.

Data in (A–D), (F–G), and (I–R) were repeated three times.

See also Table S1.

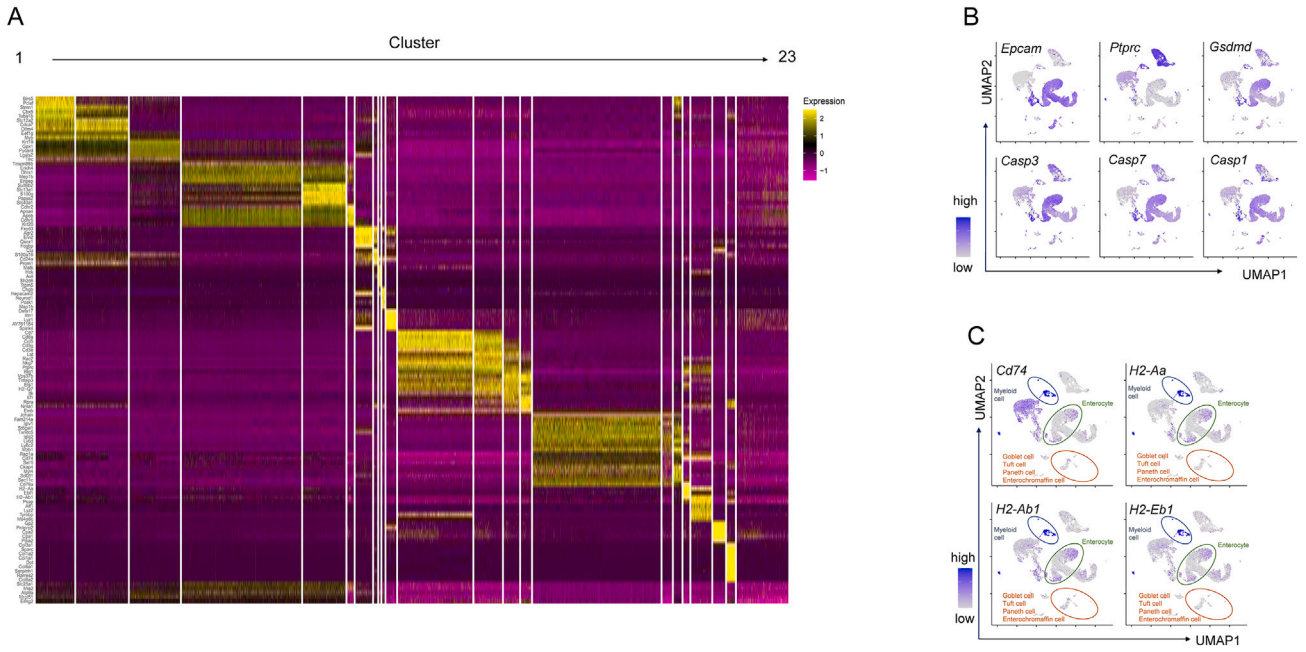


*(legend on next page)*

**Figure S4. The nuclear-localized GSDMD fragment regulates MHCII in IECs to induce Tr1 cells, related to Figure 4**

(A–C and H) Single-cell RNA sequencing of upper intestine cells from *Gsdmd*$^{SICR}$ mutant mice and littermate WT mice. Gene signatures of different subsets (A). The gene expression patterns of *Epcam* (gene encode EpCAM, marker of IEC), *Ptprc* (gene encode CD45, marker of IEL/LPL), *Gsdmd*, and *Casp-1/3/7* (B). The gene expression patterns of MHCII molecules (C). The composition of immune cell populations (H).

(D–G) GSDMD in DC did not regulate MHCII expression. Gating strategy for CD103$^{+}$ DCs (D). FACS staining for MHCII molecule in CD103$^{+}$ DCs from the small intestine of *Gsdmd*$^{+/+}$ and *Gsdmd*$^{-/-}$ mice (E). FACS staining of MHCII in BMDCs from *Gsdmd*$^{+/+}$ and *Gsdmd*$^{-/-}$ littermates upon treatment of IFN-γ (50 ng/mL) or LPS (100 ng/mL) (F). Western blots of the GSDMD (ab219800) in bone-marrow-derived dendritic cells (BMDCs) from *Gsdmd*$^{+/+}$ and *Gsdmd*$^{-/-}$ mice (G). Data in (D–G) were repeated three times.

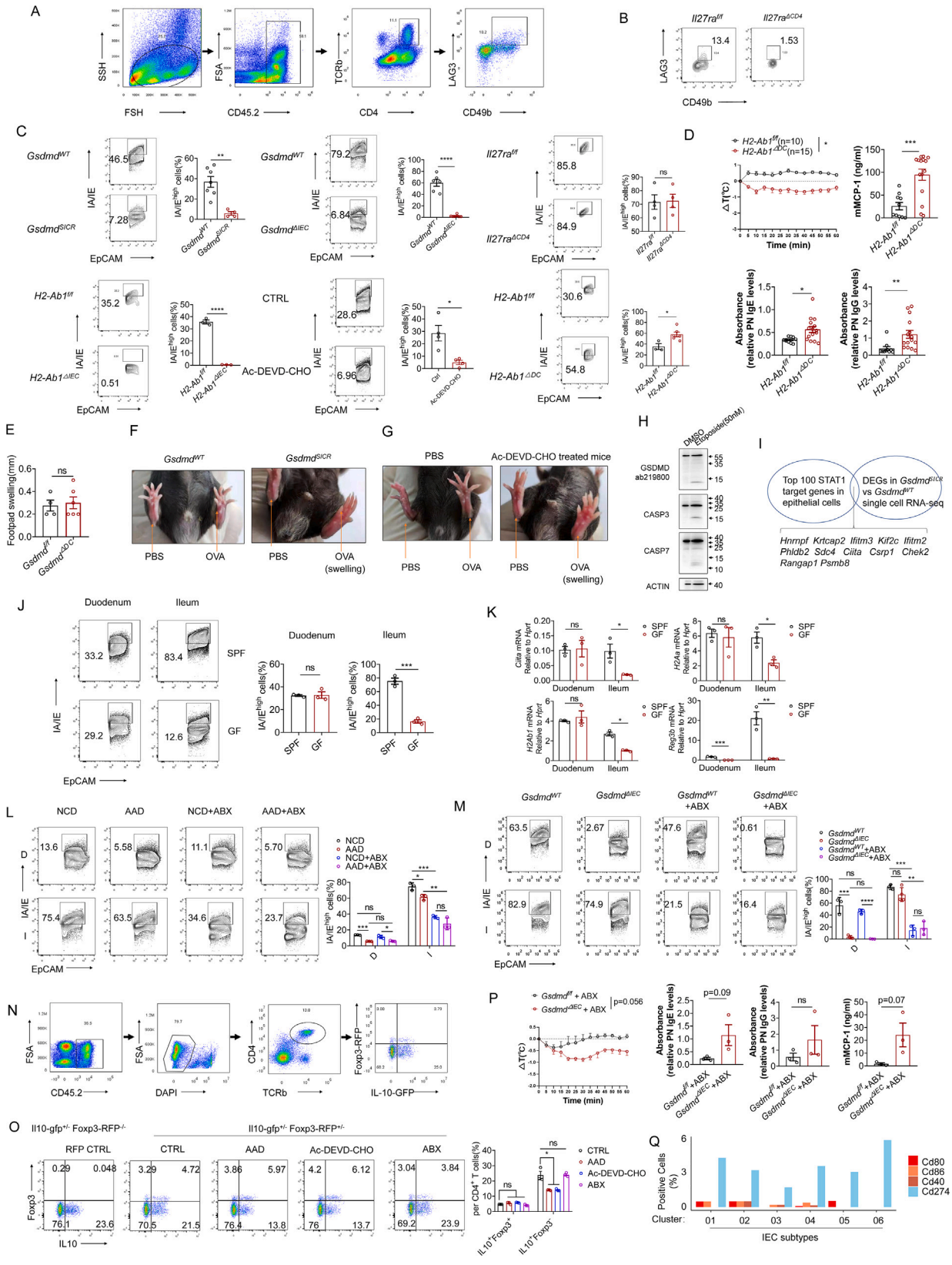

*(legend on next page)*

**Figure S5. GSDMD KO or the cleavage-resistant GSDMD variant in IECs disrupts immune tolerance to food, related to Figure 5**

(A) Gating strategy for Tr1 cells ($CD49b^+LAG3^+$) from duodenum.

(B) FACS staining of Tr1 cells ($CD49b^+LAG3^+$) in *Il27ra*$^{\Delta CD4}$ mice or WT control mice. Plots are gated from laminal propria $TCR\beta^+CD4^+$ cells.

(C) FACS staining of MHCII in duodenum IECs from indicated mice challenged by peanut allergen.

(D) Peanut allergy model. Core body temperature curve, and ELISA measurements of peanut-IgG, peanut-IgE, and mMCP-1 levels in *H2-Ab1*$^{\Delta DC}$ mice or littermate WT control mice.

(E) DTH model. Summary of footpad swelling *in Gsdmd*$^{\Delta DC}$ mice and littermate controls.

(F and G) Representative images showing footpad swelling in indicated mouse strains upon induction of delayed type hypersensitivity (DTH) model: *Gsdmd*$^{SICR}$ mice and WT littermates (F) or Ac-DEVD-CHO-treated mice and controls (G).

(H) Apoptosis induction in iBMDM. Immunoblotting of GSDMD and CASP-3/7 in BMDM cells lysates treated with apoptotic stimuli.

(I) Down-regulated STAT1 target genes in IECs from *Gsdmd*$^{SICR}$ mice compared with that from WT mice, analyzed from the aforementioned scRNA-seq dataset.

(J and K) FACS staining of MHCII (J), or qPCR detection of the expression levels of *Ciita, H2-Aa, H2-Ab1*, and *Reg3b* (K) in IECs of duodenum or ileum from SPF mice or germ free (GF) mice.

(L) FACS staining of MHCII in IECs from mice treated with AAD, ABX, or both.

(M) FACS staining of MHCII in IECs from ABX-treated or non-treated *Gsdmd*$^{\Delta IEC}$ mice or littermate control mice.

(N) Gating strategy of Tr1s ($GFP^+RFP^-$) and Tregs ($GFP^+RFP^+$) in duodenum from dual il10-GFP/foxp3-RFP reporter mice.

(O) FACS staining of Tr1s and Tregs in duodenum from dual il10/foxp3 reporter mice with indicated treatments for 1 week, Il10-$gfp^{+/-}$ Foxp3-$RFP^{-/-}$ mice were used as negative control for Foxp3-RFP signal.

(P) Peanut allergy model in *Gsdmd*$^{\Delta IEC}$ mice and littermate control mice with ABX treatment.

(Q) The expression of co-stimulatory (CD80, CD86, and CD40) and co-inhibitory (CD274, also known as PD-L1) molecules in IEC subsets from the aforementioned scRNA-seq data.

Data in (C–E), (J–M), and (O–P) are presented as the mean ± SEM, for comparisons between two groups, Student's t tests were used; for more than two groups, analysis of variance (ANOVA) was used; ns, not significant, *$p < 0.05$, **$p < 0.01$, ***$p < 0.001$, and ****$p < 0.0001$.

Data in (A–H) and (J–P) are repeated at least three times.